

**JMB**Available online at [www.sciencedirect.com](http://www.sciencedirect.com)

SCIENCE @ DIRECT®



# Interconversion of ATP Binding and Conformational Free Energies by Tryptophanyl-tRNA Synthetase: Structures of ATP Bound to Open and Closed, Pre-Transition-state Conformations

Pascal Retailleau<sup>1,2</sup>, Xin Huang<sup>1</sup>, Yuhui Yin<sup>1</sup>, Mei Hu<sup>1</sup>, Violetta Weinreb<sup>1</sup>  
Patrice Vachette<sup>2</sup>, Clemens Vonrhein<sup>3</sup>, Gérard Bricogne<sup>3</sup>  
Pietro Roversi<sup>3</sup>, Valentin Ilyin<sup>1</sup> and Charles W. Carter Jr<sup>1\*</sup>

<sup>1</sup>Department of Biochemistry and Biophysics, University of North Carolina, Mary Ellen Jones Bldg. CB# 7260  
27599-7260 Chapel Hill NC, USA

<sup>2</sup>LURE, Bâtiment 209D BP 34  
91198 Orsay Cedex France

<sup>3</sup>Global Phasing, Ltd  
Sheraton House, Castle Park  
Cambridge CB3 0AX, UK

Binding ATP to tryptophanyl-tRNA synthetase (TrpRS) in a catalytically competent configuration for amino acid activation destabilizes the enzyme structure prior to forming the transition state. This conclusion follows from monitoring the titration of TrpRS with ATP by small angle solution X-ray scattering, enzyme activity, and crystal structures. ATP induces a significantly smaller radius of gyration at pH = 7 with a transition midpoint at ~8 mM. A non-reciprocal dependence of Trp and ATP dissociation constants on concentrations of the second substrate show that Trp binding enhances affinity for ATP, while the affinity for Trp falls with the square of the [ATP] over the same concentration range (~5 mM) that induces the more compact conformation. Two distinct TrpRS:ATP structures have been solved, a high-affinity complex grown with 1 mM ATP and a low-affinity complex grown at 10 mM ATP. The former is isomorphous with unliganded TrpRS and the Trp complex from monoclinic crystals. Reacting groups of the two individually-bound substrates are separated by 6.7 Å. Although it lacks tryptophan, the low-affinity complex has a closed conformation similar to that observed in the presence of both ATP and Trp analogs such as indolmycin, and resembles a complex previously postulated to form in the closely-related TyrRS upon induced-fit active-site assembly, just prior to catalysis. Titration of TrpRS with ATP therefore successively produces structurally distinct high- and low-affinity ATP-bound states. The higher quality X-ray data for the closed ATP complex (2.2 Å) provide new structural details likely related to catalysis, including an extension of the KMSKS loop that engages the second lysine and serine residues, K195 and S196, with the  $\alpha$  and  $\gamma$ -phosphates; interactions of the K111 side-chain with the  $\gamma$ -phosphate; and a water molecule bridging the consensus sequence residue T15 to the  $\beta$ -phosphate. Induced-fit therefore strengthens active-site interactions with ATP, substantially intensifying the interaction of the KMSKS loop with the leaving PP<sub>i</sub> group. Formation of this conformation in the absence of a Trp analog implies that ATP is a key allosteric effector for TrpRS. The paradoxical requirement for high [ATP] implies that Gibbs binding free energy is stored in an unfavorable protein conformation and can then be recovered for useful purposes, including catalysis in the case of TrpRS.

© 2002 Elsevier Science Ltd. All rights reserved

\*Corresponding author

**Keywords:** tryptophanyl-tRNA synthetase; ATP-binding site; induced fit; free energy transduction; ground-state destabilization

Present addresses: X. Huang, Amgen, Suite 4700, 200 Boston Ave., Medford, MA 02155, USA; Y. Yin, Department of Molecular Biophysics and Biochemistry, Yale University, New Haven, CT 06520, USA; V. Ilyin, Biology Department, 414 Mugar, Northeastern University, Boston, MA 02115, USA.

E-mail address of the corresponding author: [carter@med.unc.edu](mailto:carter@med.unc.edu)

## Introduction

Aminoacyl tRNA synthetases (aaRSs) use the ATP hydrolysis free energy to coordinate  $\alpha$ -carboxyl group activation and acyl transfer of the appropriate amino acid to the 3'-adenosine of the cognate tRNA for protein synthesis, ensuring faithful translation of genetic information. Generally, the two processes are separable, but for GlnRS, GluRS, ArgRS, and the class I LysRS, acyl group activation requires prior tRNA binding for reasons that so far have remained unknown. Acyl group activation by ATP is so central to molecular biology that it must have been among the earliest catalytic activities to be encoded into primordial biological genomes. Indeed, the most highly conserved sequence motifs in present day aaRS are those associated with the activation step, while those involved in specific tRNA recognition appear to have accumulated later.<sup>1-3</sup> Conformational changes that coordinate amino acid activation with specific tRNA anticodon binding and intramolecular transport between activation and editing sites by editing class I aaRS likely are integrated with those associated with ATP utilization. It is therefore important to work out present-day aaRS mechanisms as deeply as possible.

Homodimeric *Bacillus stearothermophilus* tryptophanyl-tRNA synthetase (TrpRS) shares considerable structural homology with bacterial TyrRS,<sup>4</sup> the other dimeric member of subclass Ic.<sup>5</sup> Its monomer of 328 residues is the smallest among the aaRS, and includes only a minimal,  $\sim 200$  residues, implementation of the distinguishing feature of class I aaRS, which is the pair of  $\beta$ - $\alpha$ - $\beta$  cross-over connections known as the Rossmann dinucleotide-binding fold (RF) (Figure 1). The TrpRS(TyrRS) ATP pocket lies between the  $\beta$ D and  $\beta$ E strands, and the amino termini of the  $\alpha$ A and  $\alpha$ E helices, making contacts with two signature sequences, TIGN(HIGH) and KMSKS, common to all class I aaRS, and other determinants, including GxDQ at the N terminus of the  $\alpha$ E helix, that vary between the three subclasses, Ia, Ib, and Ic.<sup>6</sup> Ribose binding is mediated by the <sub>15</sub>TIGN<sub>18</sub> and <sub>144</sub>GxDQ<sub>147</sub> sequences. The absolutely invariant G17 extends a platform for the adenine base. The extended loop containing <sub>192</sub>KMSKS<sub>196</sub> provides two more determinants in TrpRS. The carbonyl oxygen atoms of I183 and M193 form hydrogen bonds (2.7 Å and 2.9 Å) to the adenine N6 amino group, precluding utilization of GTP, while the KMSKS residues constitute a distinct, PP<sub>i</sub>-binding subsite that is central to the subject here.<sup>7-9</sup>

Abbreviations used: ATP, adenosine-5' triphosphate; SAXS, small angle solution X-ray scattering; aaRS, aminoacyl tRNA synthetase; Trp, tryptophan; TrpNH<sub>2</sub>O, tryptophanamide; RF, Rossmann fold; SD, small domain; LF, ligand-free; IT, indolmycin-ATP; TAM, tryptophanyl 5' adenylate;  $R_g$ , radius of gyration; PP<sub>i</sub>, inorganic pyrophosphate; pre-TS, pre-transition state; SIR, single isomorphous replacement.

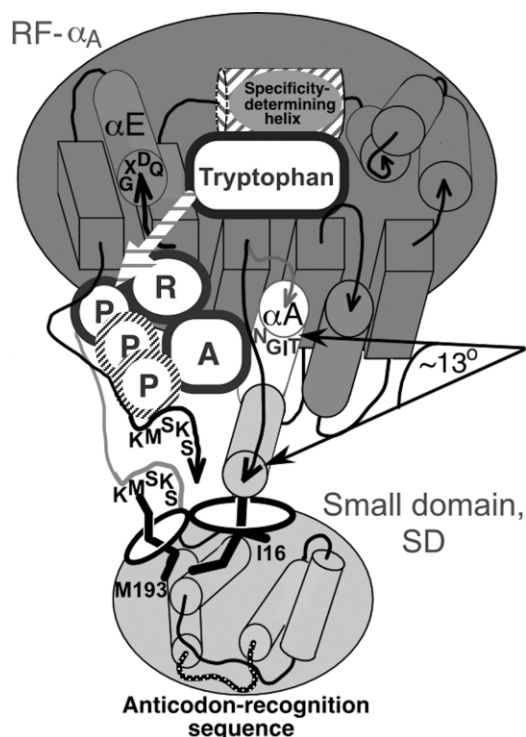


**Figure 1.** Schematic diagram of the TrpRS class Ic monomer, showing determinants of the ATP and tryptophan-binding subsites.

Crystals relevant to amino acid activation belong to two crystal families, but their structures comprise three distinct domain configurations, for which the r.m.s. differences between C $\alpha$  positions within families (0.25–0.45 Å) are up to an order of magnitude smaller than those between families ( $\sim 2.5$  Å). One crystal family includes the unliganded TrpRS (ligand-free, LF;<sup>10</sup>). This family is monoclinic, containing either three dimers per asymmetric unit (space groups  $P2_1$  and C2) or triclinc with six dimers per asymmetric unit (space group  $P1$ ). In all such crystals, packing obeys a  $3_2$  non-crystallographic screw axis. The other two conformations belong to the second, tetragonal crystal family, in which TrpRS dimers pack along a  $4_3$  screw axis with a monomer in the asymmetric unit, thereby imposing crystallographic twofold symmetry on the enzyme dimer. They have different unit cell dimensions.

Many, if not all allosteric states relevant to the TrpRS catalytic mechanism have now been solved. In particular, the structures described here now afford comparison of independent crystal structures corresponding to each state in Fersht's well-known random, bi-bi kinetic scheme (Figure 2), providing the most complete set of distinct conformational isomers yet achieved for an aaRS.<sup>4,10-14</sup> All structures were solved at near physiological pH values, and therefore should be relevant to catalysis. However, the strongest arguments in favor of their functional relevance arise from the detailed consistency of what we see

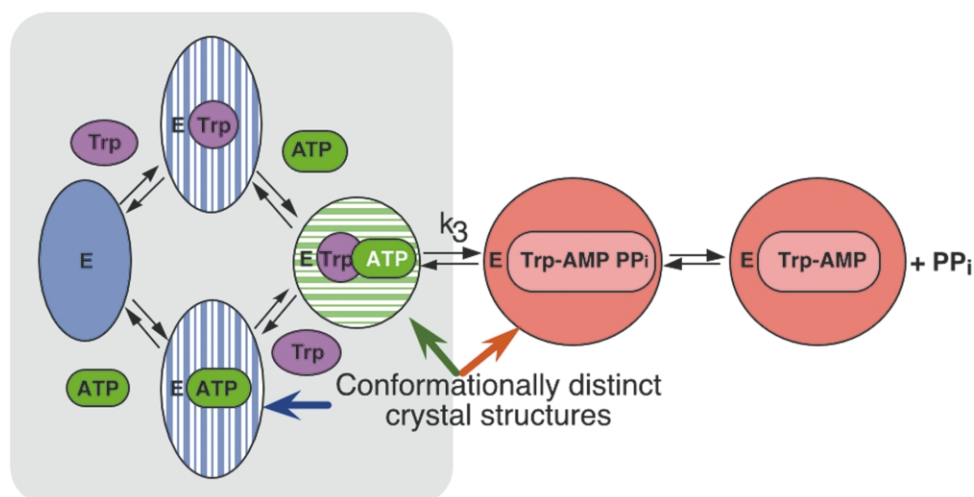


**Figure 2.** Random, bi-bi kinetic scheme developed by Fersht and colleagues for TyrRS. TrpRS structures corresponding to all states related to tryptophan activation have now been solved, and correspond in detail to those envisioned by the earlier work on TyrRS. This paper deals in particular with new structures (striped) and the relationships they suggest for the early, pre-TS processes (gray shading).

in the structures and steady-state kinetics with what was previously observed in mutagenic and pre-steady state kinetic analysis of TyrRS.

Fersht and co-workers<sup>15–19</sup> identified three groups of mutants corresponding to separate binding subsites within the RF. Pre-steady state kinetic analysis showed that mutants in different subsites affect binding affinity,  $\Delta(\Delta G)$ , differently during catalysis. Those involving amino acid binding affect the Michaelis complex, transition state, and product to the same extent, whereas those interacting either with the adenosine or  $PP_i$  have no effect until the transition-state is reached. Such differential binding of ATP in the transition-state implies relative structure rearrangements that alter binding preferences during catalysis, but no such movement had been observed in any class I aaRS structures until the open, unliganded TrpRS structure.<sup>10</sup>

Structural comparison revealed that the  $\alpha A$  helix from the RF forms a separate small domain (SD) with a 4-helix bundle C-terminal to the RF.<sup>4,10</sup> Thus, ATP-binding determinants lie at the interface between two functionally separate domains, which are linked *via* two “belts”, or short peptide segments that allow coordinated relative motion of the two domains. In open complexes, the SD rotates away from the  $\alpha E$  helix and GxDQ sequence, fragmenting the ATP-binding site into two parts.

Here, we describe several new structures that allow us to address the thermodynamic linkage between nucleotide binding and conformational equilibria in class I aaRS from a structural standpoint, using TrpRS as a model system. We have titrated TrpRS with both Trp and ATP using three different measurements, each suggesting that ATP binding to TrpRS is bimodal and linked to conformational changes. (i) Small angle X-ray scattering

shows an [ATP]-dependence of the radius of gyration ( $R_g$ ). (ii) Kinetic assays show unexpected, ATP-induced changes in Trp-affinity. (iii) Bimodal ATP-binding behavior is confirmed by the structures of two binary distinct TrpRS:ATP complexes. One of these, formed only at high [ATP], is very similar to the closed structures observed previously only in abortive ternary complexes with ATP plus indolmycin (indolmycin-ATP, IT<sup>13</sup>), tryptophanol (X.H., unpublished results), tryptophanamide, described here, and other non-reactive Trp analogs. This narrowly defined family of structures has all of the properties expected for a closed, pre-transition state (pre-TS) complex predicted by Fersht.<sup>18</sup> Titration with Trp provides no evidence for conformation changes.

The close coincidence of all [ATP]-dependent titrations suggests answers, for the first time, to three interrelated questions about the energetics of induced-fit mechanisms in class I aaRS:

- What interactions convert the open, ground state TrpRS structure into the closed, pre-TS complex and, conversely, what maintains the open conformation in the absence of substrates?
- What weakens ATP binding as the active site assembles?
- What is the relationship between induced-fit and catalysis?

Answering these questions highlights the central role of ATP in the mechanism of amino acid activation by class I aaRS, suggesting that the induced-fit interaction with ATP may be inherently destabilizing to protein conformations of all class I aaRS. Important new analogies appear between them and other transducing enzymes that use the potentially high nucleoside triphosphate-binding

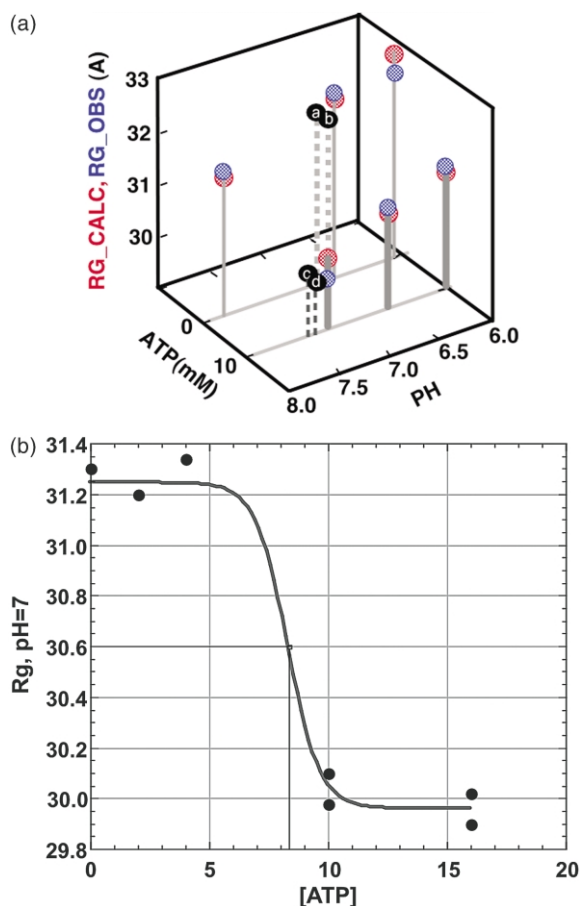


**Figure 3.** ATP and pH-dependence of TrpRS conformation on the basis of SAXS measurements of the radius of gyration and crystal structures. (a) Bivariate modeling. Blue spheres represent averages of  $\sim 9$  determinations of  $R_g$  under conditions indicated by their position on the two-dimensional plan. Red spheres represent  $R_g$  values calculated from the bivariate model in Table 1:  $R_{g,calc} = 32.52 - 1.8[ATP] - 0.8 pH_{relative}$ . Black spheres represent calculated  $R_g$  values on the basis of crystallographic coordinates for LF TrpRS at pH = 6.8 (a), the open ATP complex reported here (b), the trp-5'-AMP complex at pH = 7.5 (c), and for the closed ATP complex reported here (d). (b) Titration of TrpRS with ATP at pH = 7.0, showing the midpoint [ATP] required to shift the  $R_g$  from that of the open to the closed form. The fitted curve is a sigmoid of the form  $y = A_2 + A_1 - A_2/1 + \exp^{(x-x_0)/dx}$ , where  $A_2$  and  $A_1$  are the initial and final values,  $x_0$  is the midpoint, and  $dx$  the width of the transition. The fitted midpoint is at [ATP] = 8.3 mM.

affinity to interconvert the highly exergonic phosphate ester hydrolysis in aqueous solution and useful forms of work and information.

## Results

### The TrpRS radius of gyration in solution is reduced by high [ATP] and high pH

Small angle X-ray scattering (SAXS) can be used to determine radii of gyration ( $R_g$ ) for biological macromolecules in solution, and in particular, how they vary as functions of relevant experimental parameters. A detailed factorial study of the TrpRS  $R_g$  was carried out in order to verify the extent to which conformational changes observed in crystals were consequences of solution parameters and hence not imposed by crystal packing constraints. Multiple samples were analyzed on a factorial experimental plan similar to that originally used to characterize TrpRS crystal growth.<sup>20,21</sup>

The difference between  $R_g$  for the LF structure and the Trp5'-AMP complex (32.5 Å versus 30.2 Å) was previously shown to be significantly higher than the standard deviation of the measurements.<sup>10</sup> In fact, in the phosphate buffer used to crystallize TrpRS both pH and ATP concentration affect TrpRS  $R_g$  values significantly (Figure 3(a)). Compact TrpRS structures in solution result from high levels of [ATP] (10 mM) and high levels of pH (7.5). Moreover,  $R_g$  values for TrpRS in solution match closely with those calculated from crystallographic coordinates obtained under corresponding conditions. In particular,  $R_g$  values for the open and closed ATP crystal structures (b and d) are similar to those for the LF and adenylate complex structures (a and c), respectively, showing in both cases a reduction of  $\sim 2.0$  Å in the presence of high [ATP].

Statistics of the bivariate modeling in Table 1 document the significance of both predictors. Trp is not a significant predictor in any multivariate model for  $R_g$  (Student *t*-test probability = 0.13).  $R_g$  values calculated from coordinates show a consistent and significant difference between pre-TS ( $\langle R_g \rangle = 29.64 \pm 0.17$  Å) and product ( $\langle R_g \rangle = 30.11 \pm 0.12$  Å) states. These differences are within

**Table 1.** Bivariate dependence of radius of gyration on ATP and pH. ATP is a binary variable, + or -. pH is a continuous variable given relative to the mean pH of the experimental plan. The dependent variable is  $R_g$ . A total of 54 independent measurements were made. The squared multiple regression coefficient,  $R^2$  is 0.702

Variable	Coefficient	Standard Error	<i>t</i>	P(2-TAIL)	
Constant	32.52	0.118	275.0	$1.0 \times 10^{-15}$	
ATP	-1.75	0.160	-10.9	$6.1 \times 10^{-15}$	
PH_REL	-0.83	0.145	-5.7	$5.4 \times 10^{-7}$	
<i>Analysis of variance</i>					
Source	Sum-of-squares	DF	Meansquare	<i>F</i> -ratio	<i>P</i>
Regression	32.217	2	16.109	59.975	$4.03011 \times 10^{-14}$
Residual	13.698	51	0.269		

the experimental error, however, so the SAXS data do not distinguish between them. The consistency of molecular dimensions in solution with those from the crystal structures, the small Student *t*-test probabilities for ATP ( $6.1 \times 10^{-15}$ ) and pH ( $5.4 \times 10^{-7}$ ) as predictors, and pH optima of 7.5 for tetragonal and 6.7 for monoclinic crystal growth determined from response-surface experiments<sup>10,22</sup> together comprise convincing evidence that adenine nucleotide binding is a primary molecular determinant of TrpRS conformation and that crystallization does indeed trap a dominant species from a bivariate pH and [ATP]-dependent distribution in solution.

The pHs in these experiments fall in a physiological range, while ATP concentrations exceed physiological values. We should therefore distinguish here and elsewhere between results we interpret to be physiologically relevant and others that are useful for their physicochemical import. The high level of [ATP] required for closure of the TrpRS active site in the absence of Trp ( $\sim 8$  mM; Figure 3(b)) falls into the latter category, as evidence in the next section shows that the structure formed is an abortive complex that does not bind Trp. The concentration required for this conformational change is, however, relevant to considerations of the internal conformational and binding thermodynamics.

### Factorial studies of PP<sub>i</sub>-exchange kinetics show non-reciprocal cooperativity between ATP and Trp

That ATP is a conformational trigger is illustrated further by comparing how affinities for Trp and ATP obtained from pyrophosphate (PP<sub>i</sub>) exchange kinetics<sup>†</sup> change with the order of substrate addition and the relative concentrations of the second substrate. If kinetically relevant conformation changes are involved in catalysis, as is evidently the case for TrpRS, then differential

binding of substrates to different conformational states can introduce ambiguity in the interpretation of kinetic experiments performed at a single combination of substrate concentrations. Similarly, measurements at single substrate combinations may reveal differences, but fail to suggest how the system responds as substrate concentrations change.

The order of substrate addition has an important influence (Figure 4(a) and (b)). Pre-incubation of TrpRS with subsaturating [ATP] significantly stimulated PP<sub>i</sub> exchange at low [Trp] (Figure 4(b)). We conclude that prior interaction with ATP favors the induced-fit, changing the state of the enzyme and somehow facilitating exchange once the amino acid is provided.

Michaelis–Menten PP<sub>i</sub> exchange kinetics were therefore measured in triplicate using both orders-of-addition for a series of concentrations of each substrate at different concentrations of the other substrate according to a factorial design, Table 2, that is experimentally similar to those used to differentiate between random and sequential binding order.<sup>23</sup> Each factorial grid of measurements was analyzed by fitting Michaelis–Menten parameters for each substrate, Figure 4(c) and (d), to determine the bivariate dependence of exchange rates on the two substrate concentrations. In the present case we are interested in functional relationships between the kinetic parameters, which in themselves suggest how the data relate to conformation change. As with other applications of factorial designs,<sup>24</sup> the analysis reveals synergistic effects between the two ligands, the most salient of which are shown in Figure 4(e) and (f). Experiments of Fersht<sup>25</sup> provide similar information for TyrRS.

Preincubation with increasing [Trp] enhances TrpRS affinity for ATP (Figure 4(e)). Synergistic binding effects are expected for enzymes that catalyze two-substrate reactions. The magnitude of the interaction is quite weak, however, as will be discussed further below.

The surprising result, Figure 4(f), is that we do not observe the converse effect. Higher ATP concentrations lead instead to substrate inhibition and hence to increasing  $K_{i,W}$  values for Trp. Of particular interest, the decrease in Trp affinity is proportional to the square of the ATP concentration, implying participation of two molecules of ATP in the process that weakens Trp affinity in the kinetic assay. The natural inference is that binding of an ATP molecule to both active sites in the TrpRS dimer somehow limits access of tryptophan to its binding site. Exclusion of tryptophan by binding two moles of ATP per dimer cannot be an equilibrium binding interaction, because the binding of tryptophan actually promotes ATP binding (Figure 4(e)). From thermodynamic linkage,  $\delta\langle y_{\text{Trp}} \rangle / \delta \ln[\text{ATP}] = \delta\langle y_{\text{ATP}} \rangle / \delta \ln[\text{Trp}]$ , the effects should be reciprocal.

Significantly, the [ATP] range of this effect, 0.5–5 mM, is well above the  $K_d$  for ATP, which is

<sup>†</sup> PP<sub>i</sub> exchange occurs under equilibrium binding of both tryptophan and ATP, so the fitted half-saturation values represent thermodynamic dissociation constants.<sup>95</sup> In keeping with Cleland's recommendations (W.W. Cleland, personal communication), we will refer to the fitted half-saturation values as  $K_{i,T}$  and  $K_{i,W}$  and maximum exchange rates as  $k_{\text{max},T}$  and  $k_{\text{max},W}$  respectively. This question remains a source of contention, dating as far back as the early 1970s<sup>96</sup> suggests that the interpretation of half-saturation values as dissociation constants is strictly valid under the extremes of the conditions we have used in these experiments, i.e. when the half-saturation value of one substrate is determined at very subsaturating concentrations of the other. Our use of Cleland's analysis is supported by the fact that the binding of ATP is weak enough at these extreme values (i.e. 2  $\mu\text{M}$  Trp) that its off rate greatly exceeds the rate of the forward reaction. Thus, as the affinity for ATP decreases as the TrpRS active site closes, the interpretations we place on  $K_{i,W}$  are approximately correct throughout the range.

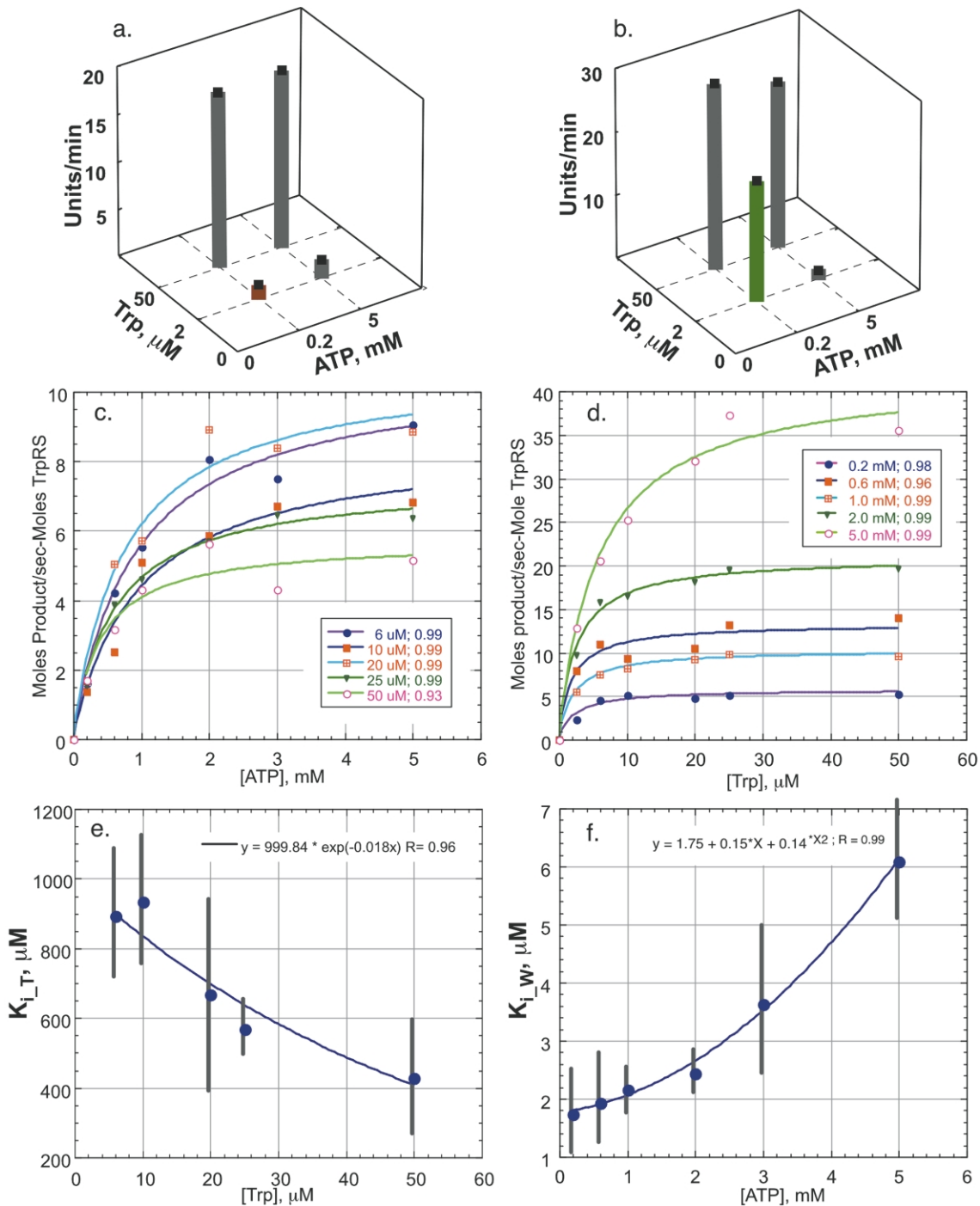


**Figure 4.** Factorial analysis of PP<sub>i</sub> exchange kinetics. (a) and (b) Order of addition experiments. Enzyme was preincubated 30 minutes with the indicated concentrations of Trp (open state; (a)) or ATP (pre-TS state, (b)), and the reaction was initiated by adding the indicated concentrations of the second substrate. (c) and (d) [ATP] and [Trp] dependencies of exchange rates for TrpRS preincubated with varying amounts of Trp (c, e) and [ATP] (d, f) and initiated with different concentrations of the second substrate. All points are in moles product/sec-moles-enzyme. (e)  $K_{i,T}$  versus [Trp] for TrpRS initially in the open state. (f)  $K_{i,W}$  versus [ATP] initially or partially in the pre-TS conformation.

**Table 2.** Factorial kinetic assays of the bivariate dependence of <sup>32</sup>PP<sub>i</sub> exchange on [Trp] and [ATP]

Substrate						
Trp (μM)	2.5	6.0	10.0	20.0	25.0	50.0
ATP (mM)	0.2	0.6	1.0	2.0	3.0	5.0

~0.4 mM<sup>26,27</sup> and coincides with the ATP concentrations required for maximal decrease in the  $R_g$  of the TrpRS dimer, and for growth of the tetragonal TrpRS crystals whose structure is reported here. That structure therefore affords a rationale for the quadratic ATP-dependence, showing that ATP binding to both subunits induces a closed TrpRS

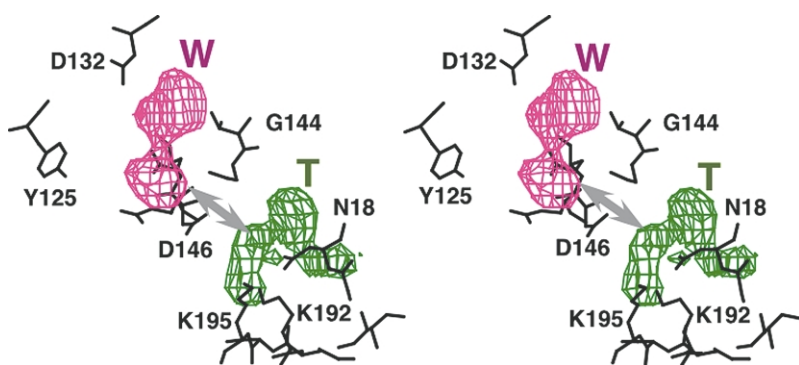


**Figure 5.** Composite  $[F_{\text{obs}} - F_{\text{calc}}]$  maps showing the relative locations of bound substrates tryptophan (W; magenta) and ATP (T; green). The relevant distance between reactive groups involved in tryptophan activation is indicated by the gray arrow, and from refined coordinates is 6.7 Å.

conformation that is unable to bind Trp directly, and TrpRS must first revert to the open configuration to provide access to the Trp-binding site.

The maximum exchange rate,  $k_{\text{max},W}$ , is independent of [Trp], but increases sharply with [ATP] (not shown), consistent with a role for ATP, but not tryptophan, in the induced-fit assembly of the active site. The offsetting effects of ATP increase both  $k_{\text{max},T}$  and  $K_{i,T}$ . Thus, the apparent second-order rate is relatively independent of [ATP] up to quite high [ATP] levels, but increases significantly with respect to [Trp].

### Twofold symmetry and the apparent structural invariance of the TrpRS dimer interface

Before turning to the structural data, we note that TrpRS and TyrRS are functionally obligate dimers. The open Trp and ATP complexes described here are asymmetric in the manner observed for LF TrpRS structures, which display different SD orientations within each dimer;<sup>10</sup> the closed ATP complex appears to be symmetrically liganded with one ATP per monomer. The symmetrically liganded Trp-5'AMP complex, despite crystallographic twofold symmetry, is obtained from an asymmetrically-liganded crystalline intermediate with two moles of  $^{14}\text{C}$ -Trp and one mole of  $^{32}\text{P}$ -ATP<sup>28</sup> per dimer when phosphate is replaced by sulphate.<sup>13</sup> Thus, there is strong crystallographic evidence that TrpRS is an asymmetric dimer under most circumstances.

Asymmetry was observed in solution for TyrRS.<sup>29,30</sup> Enzymatic<sup>31</sup> and structural observations<sup>32,33</sup> argue that domain movements in response to ligand binding must be coordinated *via* intersubunit communication, their active sites being  $>45$  Å apart. Further, interchanging the identities of tRNA<sup>Gln</sup> and tRNA<sup>Trp</sup> by anticodon mutations primarily effects  $k_{\text{cat}}$ <sup>34,35</sup> so correct anticodon binding to one monomer somehow initiates aminoacylation of the acceptor stem bound to the second monomer. However, the only indication of molecular asymmetry in the closed ATP complex is the mutually exclusive hydrogen-bonded configurations of the two, symmetry-related, Q94 side-chains across the molecular dyad identified

previously in the product complex.<sup>14</sup> We cannot trace intersubunit communications during the catalytic cycle, however, because the dimer interface is nearly invariant in all three structural families. Thus, we will focus in the following sections on the three binding subsites of the TrpRS monomer—amino acid, ribose, and PP<sub>i</sub>—whose catalytic roles were differentiated by Fersht's work on TyrRS.<sup>15–18</sup>

### Neither tryptophan nor low ATP concentrations alter the open, unliganded TrpRS conformation†

Crystals were prepared at pH = 6.6 by co-crystallization of TrpRS with either 2 mM Trp ( $1000 \times K_m$ ) or 1 mM ATP ( $2.5 \times K_m$ ). Both monoclinic crystals are essentially isomorphous to monoclinic LF TrpRS,<sup>10</sup> and were solved by molecular replacement. They provide putative structural representations of the three corresponding states in Fersht's kinetic scheme (Figure 2). Thus, for TrpRS, these states all have the same, open tertiary structure. Protein atoms in all three independent dimers superimpose uniquely and unambiguously in all three structures, so we can construct the combined representation of the two ligand-bound states as shown in Figure 5. The  $\alpha$ -phosphate is 6.7 Å away from the Trp carboxylate oxygen in the corresponding Trp complex, precluding reaction between them in this conformation.

In each single-ligand complex the substrates occupy subsites identified in previous work. Trp binds between F5, M129, D132, and V141. ATP binds to the TIGN and KMSKS signatures in the outer SD, which is rotated away from the RF as in the LF structure,<sup>10</sup> making few contacts with the main body of the RF. Superposition of open ATP and Trp TrpRS complexes reveals very small r.m.s. deviations (0.67 Å for all 8500 atoms) in the three dimers in the asymmetric unit. Thus, neither substrate changes the molecular asymmetry of the open conformation.

† PDB ID codes: Open Trp complex, 1MB2; Open ATP complex, 1MAW; Closed, pre\_TS ATP complex, 1M83; Closed, pre-TS tryptophanamide:ATP complex, 1MAU.

**Table 3.** After application of rotation/translation function in amore molecular replacement<sup>42</sup>

Searching models Structure factors range 8–4 Å	ATP Michaelis	IT pre-inter- mediate	Adenylate product
Correlation	0.096	0.633	0.277
R-factor	0.562	0.372	0.511

The open conformation binds ATP stoichiometrically† to both sites on the three dimers, with only slight variation in occupancy. There is no correlation between occupancy and hinge angle. The two active sites in the TrpRS dimer are structurally different, consistent with their having different affinities. Detailed differences between the binding of ATP to the two sites are beyond the scope of this paper, and must be investigated further, hopefully with higher resolution data.

The separate binding sites confirm our earlier suggestion<sup>10</sup> that ATP and Trp binding to the open form do not interfere with one another, and hence that the random kinetic binding order need not involve a virtual equilibrium between the E·ATP and E·Trp complexes. The generally weak or non-existent interactions with many residues that contact the adenosine moiety in the Trp-5'/AMP (TAM) complex, especially D146, S11, and Q9, is consistent with the fact that mutations of the homologous TyrRS residues have no measurable effect in ground-state complexes. Thus, the case is strong that these structures resemble on-path interactions.

### High [ATP] and high pH lead to formation of an abortive binary complex in which TrpRS assumes the pre-transition-state conformation

A second, distinctively different TrpRS:ATP complex was solved from a tetragonal crystal form grown from sodium citrate at pH = 7.5 and in the presence of 10 mM ATP. Studies of TrpRS crystal growth<sup>21</sup> suggested that tetragonal crystals grew reproducibly at high pH (~7.5) in potassium phosphate buffer from solutions containing three types of ligands: ATP plus Trp, ATP plus a non-reactive Trp analog, or high concentrations of ATP alone. The first case involved the product, Trp2' (3') ATP, synthesized by acyl transfer of Trp from the adenylate intermediate to a second ATP molecule from the medium,<sup>28</sup> and which cannot be

† The mean occupancy for ATP at both sites of all three dimers was ~0.85. The refined occupancy is a macroscopic quantity, without a direct molecular interpretation. The preferred configuration of the open complex probably binds one ATP per dimer (occupancy = 0.5) and crystal packing in the monoclinic lattice provides sufficient Gibbs energy to prevent domain closure up to a statistical threshold somewhat above this value.

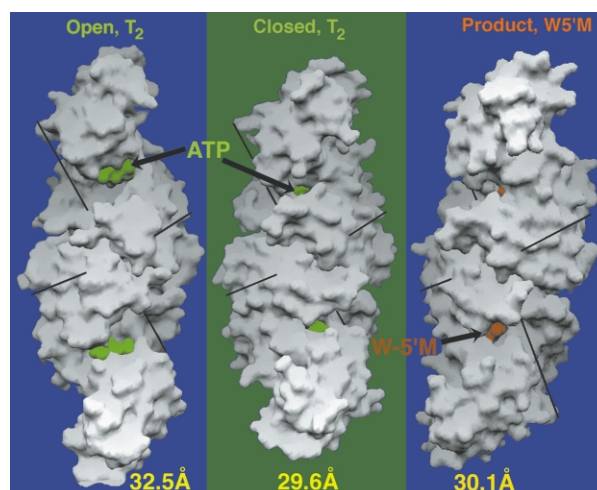


**Figure 6.** The structure of the closed, pre-TS TrpRS binary ATP complex compared with the open ATP complex and the closed, product complex containing Trp-5'/AMP. Adenine nucleotide ligands are colored green for ATP and red for tryptophanyl-5'/AMP. The figure illustrates the differences in  $R_g$  of the three TrpRS conformational states, as well as the domain rearrangements within the monomer. The two closed states can be differentiated relative to the internal orthonormal coordinate system; the product complex fully reveals the axis on the lower right.

visualized because it is disordered.<sup>13</sup> Adenylate resynthesis can be promoted after transfer of these crystals to ammonium sulfate,<sup>4</sup> and leads to a modest decrease (61 Å versus 63 Å) along the *a* and *b* unit cell axes. The second case, prepared with non-reactive Trp analogs, produces crystals with a shorter *c* axis compared to those grown with both substrates (217 Å versus 232 Å) in order to accommodate a substantial reorientation of the SD. Furthermore, these crystals are unchanged when transferred to ammonium sulfate. The third case involved ATP without a tryptophan subsite ligand. The same [ATP], ~10 mM, was used to grow all tetragonal ATP complex crystals.

Titration of TrpRS with ATP without Trp analogs therefore shows a comparable midpoint of ~5 mM at pH 7.5<sup>21</sup> for transition between monoclinic and tetragonal crystal forms and for the decrease in  $R_g$  from 32 Å to 29.5 Å in solution. This concentration is roughly two orders of magnitude higher than the TrpRS concentration present in crystallization conditions, 140 μM, and that required to saturate the active site for catalysis ( $K_{d,ATP}$  for PP<sub>i</sub> exchange ~400 μM). The switch from monoclinic to tetragonal crystals at higher pH, just by increasing [ATP], verifies and reveals the nature of the conformational change triggered by ATP binding.

Comparative molecular replacement solutions (Table 3) used to initiate phasing with native structure factor amplitudes between 8 Å and 4 Å show, unambiguously, that the 10 mM ATP-dimeric complex presents the most compact of the three TrpRS conformational families (Figure 6).

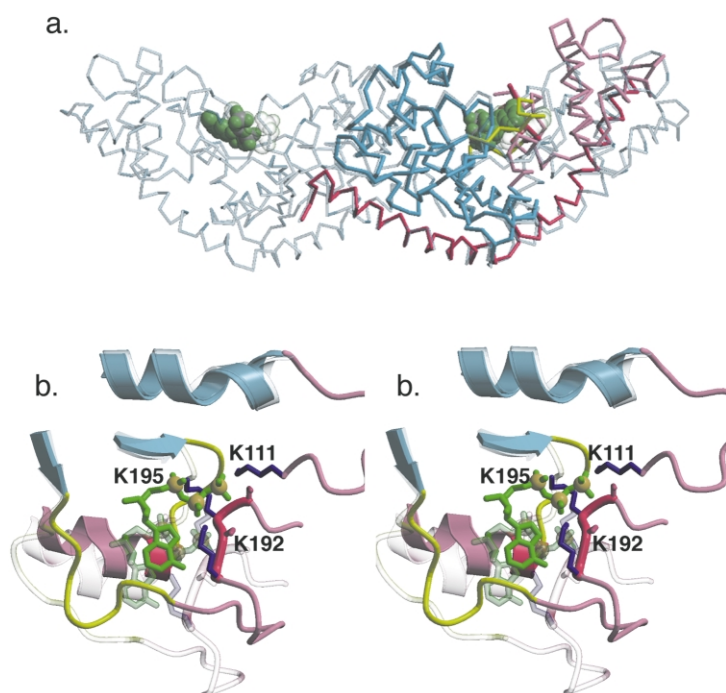


**Figure 7.** Assembly of the ATP-binding site by domain movement, superimposing the assembled ATP-binding site on the open ATP complex (semitransparent) conformation. (a) Dimeric TrpRS. (b) Active site. Blue: Rossmann fold domain, RF- $\alpha$ A. Red: small domain and C-terminal helix, SD. Green: ATP bound to the closed conformation described in this work. Yellow: long and short belts whose  $\{\phi, \psi\}$  angles change substantially to facilitate domain motion. Dark blue: the three lysine residues that interact with the  $PP_i$  leaving group.

The conformation is characteristic of the closed pre-TS biochemical state.<sup>13</sup> The final overall r.m.s. coordinate difference between the 10 mM ATP complex and the IT complex starting model, is 1.2 Å (0.6 Å for the backbone)<sup>†</sup>.

### Domain movements assemble the ribose and $PP_i$ -binding subsites

The open ATP complex shows that ATP can use the distal half of the active site to bind stably to the open conformation adopted by the LF structure. The extended SD configuration removes the  $\alpha$ A helix with the two signature sequences and long belt 175–182 from their proximity to the active site, resulting in a  $>4$ –6 Å separation of the two complementary parts of the ribose-binding site (Figure 7(b)). The ribose moiety interacts only with the N18 (TIGN) amide nitrogen in the “open” ATP complex, the GxDQ determinant remaining with the structurally conserved part of the RF, and losing contact with the ribose moiety. As in the closed complexes described here, however, the adenine moiety in the open complex is recognized by the backbone carbonyl groups

of M193 and I183, and also by G17 (TIGN). K192 ( $\epsilon$ - $NH_3^+$ ) interacts with the  $\beta$ -phosphate forming the only side-chain interaction between the  $PP_i$  and the KMSKS loop, which binds incompletely in the open conformation (Figure 14(a)), and will be discussed separately in a subsequent section.

Increasing [ATP] at higher pH rejoins the two fragments of the ATP-binding pocket, allowing interaction of the ribose moiety with the GxDQ determinant and completing the ribose-binding subsite. It is mediated by rotation of the  $\alpha$ A helix, accompanied as a rigid body by the SD, back toward the RF (Figure 7), almost exactly as observed in the IT complex.<sup>13</sup> The domain movement brings the  $\alpha$ -phosphate from a position 6.7 Å away to within only 3.4 Å from the Trp carboxylate oxygen atom, positioning the  $\alpha$ -phosphate in the latter in a nearly ideal position for in-line attack by the carboxylate of the amino acid substrate (Figure 9). The domain movement is consistent with the decreased  $R_g$  measured in solution by SAXS, but leads to a conformation distinct from that of the Trp-5' adenylate complex.<sup>4,14</sup>

The adenine moiety is buried in the open ATP complex, but considerable fractions of ribose and  $PP_i$  surface areas remain solvent accessible. Domain closure reduces solvent accessibility essentially to zero (Figure 8(b)). The triphosphate moiety remains in the usual, bent conformation in both open and closed ATP complexes. The ribose 2'-OH group forms a good hydrogen bond (2.6 Å) with the carboxylate group of D146 in the GxDQ determinant of the  $\alpha$ E-helix (Figures 1 and 15).

TrpRS requires a single  $Mg^{2+}$  ion for  $PP_i$ -exchange, and the  $[Mg^{2+}]$  necessary for half-saturation is  $\sim 2.0 \mu M$  (Figure 10(a)). The only

<sup>†</sup> Discrepancies likely reflect both the variation of temperature between experimental conditions (100 K versus 300 K) and the significantly improved resolution limits (2.2 Å versus 2.9 Å). Numerous beta-branched residues had to be repositioned in the ATP 2.2 Å structure and side-chains on the surface displayed different rotamers. The conspicuously different backbone regions are in the short belt (10–12), one of the two flexible peptide links that ensure coordination of domain movements, and the usual disordered loop, 110–117, that recognizes the 3'-acceptor terminus of tRNA<sup>Trp</sup>.

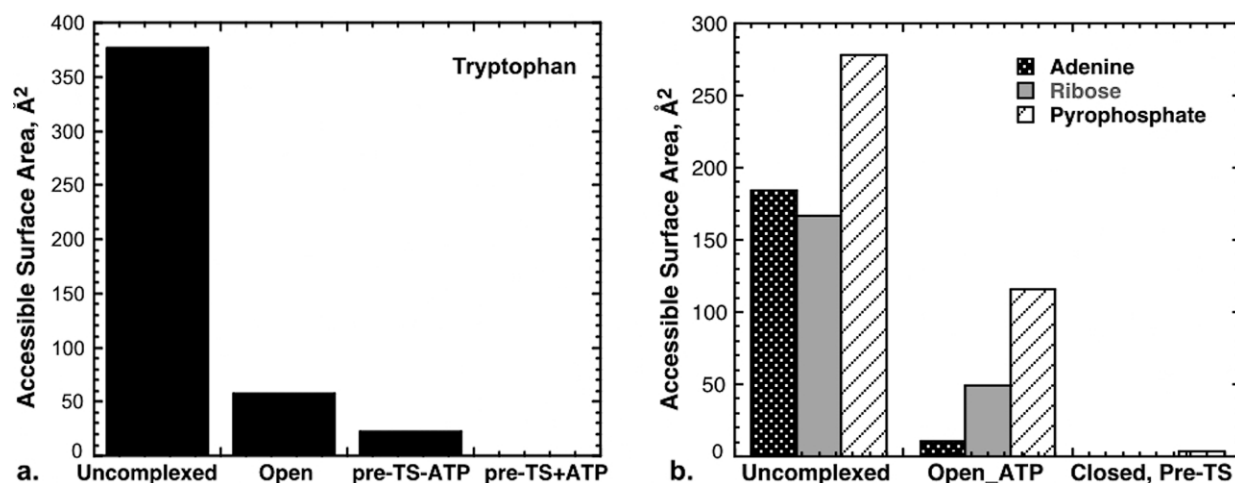


**Figure 8.** Progressive enclosure of substrates Trp (a) and ATP (b) in the TrpRS conformational cycle. Both substrates become totally enveloped in the closed, pre-TS complex. Tryptophan complexes are illustrated both in the presence and absence of ATP to show the restriction induced by rotation of Y125, Q9, and Q107 (Figure 9). Adenine, ribose, and PP<sub>i</sub> are plotted separately to emphasize that the adenine moiety is essentially sequestered in the open complex, leaving the PP<sub>i</sub> proportionately the most exposed.

reasonable site for Mg<sup>2+</sup> binding is a spherical, 8σ electron density peak within 2.2 Å < d < 2.7 Å from oxygen atoms of each ATP phosphate group (Figure 11). Attempts to replace Mg<sup>2+</sup> by Mn<sup>2+</sup>

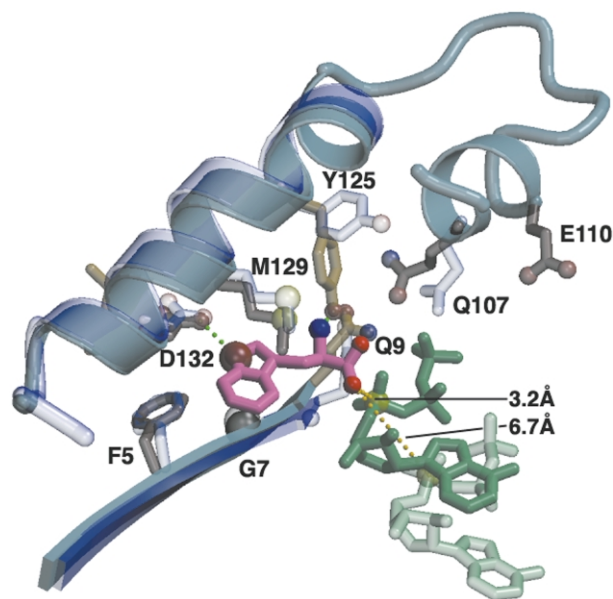


**Figure 9.** Coordinated rotations of Y125, Q9 and Q107 at the mouth of the Trp-binding subsite from their positions in the open states induced by ATP binding. Trp is placed in the structure in accordance with its position in the open Trp complex. The large, semi-transparent red sphere at the site of the indole nitrogen atom of the substrate is the location of water W528 in the closed, binary ATP complex. Relative positions are shown for ATP in the open (transparent) and closed, pre-TS (fully rendered) complexes. Active-site assembly brings the α-phosphate from 6.7 Å to within 3.2 Å of the Trp carboxylate oxygen. Most dramatic of the coupled motions in the Trp pocket is that of the highly conserved residue, Y125. Structure superposition in this and other figures is described in Materials and Methods.

for more definitive crystallographic evidence regarding this peak have not produced any Mn<sup>2+</sup> derivative crystal complexed with either ATP or AMP + PP<sub>i</sub>, irrespective of the crystallizing salt used, phosphate, sulfate, or the stronger chelator, citrate. Moreover, activity is reduced tenfold with Mn<sup>2+</sup>, suggesting that it does not substitute readily for Mg<sup>2+</sup> (Figure 10(b)), perhaps because its constrained environment cannot easily accommodate Mn<sup>2+</sup>. The Mn<sup>2+</sup> ionic radius, 0.74 Å, is 14% larger than that of Mg<sup>2+</sup>, 0.65 Å, but Mn<sup>2+</sup> is often a functional active site substitution for Mg<sup>2+</sup> that maintains the catalytic efficiency of magnesium-utilizing enzymes.<sup>36</sup> We tentatively conclude that this peak represents a bound Mg<sup>2+</sup>.

TrpRS itself provides no ligands to this group, which binds only to three phosphate oxygen atoms and two water molecules (Figure 12(a)). *Ab initio* molecular orbital calculations indicate that five-coordinated Mg<sup>2+</sup> lie 6.4 kcal/mol higher in energy than the fully six-coordinated species.<sup>37</sup> Moreover, they usually form distorted bipyramidal configurations as observed in the A-site Mg<sup>2+</sup> of polymerases.<sup>38</sup> The energy cost of the atypical TrpRS deficient octahedral coordination sphere suggests a possible functional significance. The O<sup>δ1</sup> carboxylate oxygen of D146 (4.1 Å) and the N<sup>δ2</sup> amide nitrogen of Q147 (4.3 Å) are close enough to join its coordination sphere if, for example, the Mg<sup>2+</sup>, perhaps together with PP<sub>i</sub>, were to move toward them during phosphoryl-transfer.

### Conformational activation by ATP does not require tryptophan pocket ligands

The final  $\{|F_{\text{obs}}| - |F_{\text{calc}}|, \Phi_{\text{refined, LF model}}\}$  map, contoured at 4σ (Figure 13(a)) shows density for ATP and two peaks within the Trp-binding pocket that were modeled as water molecules. Substituting the indole pocket M129 with the more

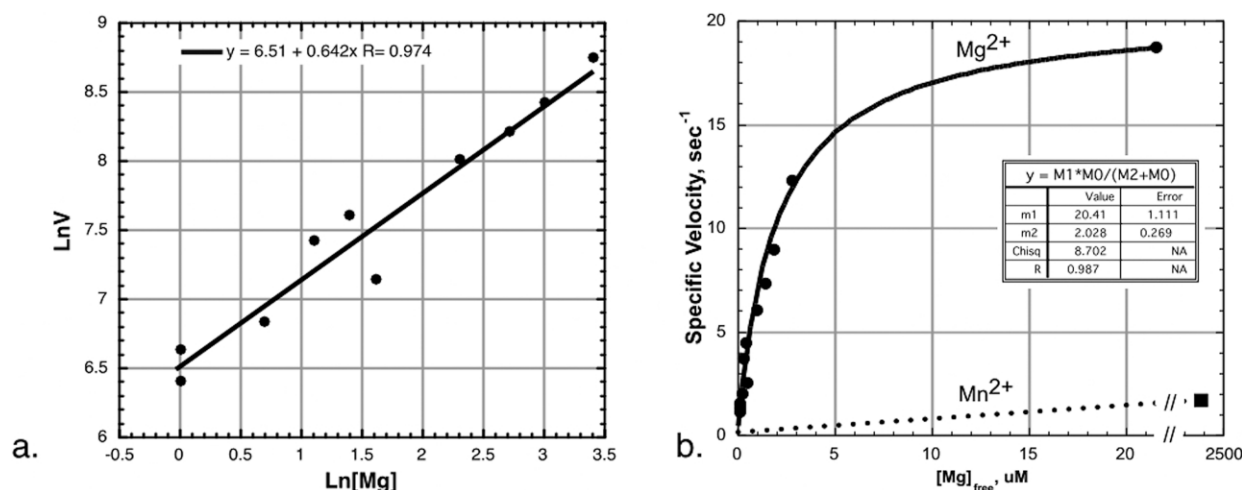


**Figure 10.** Mg<sup>2+</sup>-dependence of TrpRS amino acid activation. (a) Molecularity of the reaction. A single Mg<sup>2+</sup> appears to be required for catalysis of tryptophan activation. (b) Michaelis–Menten plot showing saturation behavior and suggesting an affinity of  $\sim 2.0$   $\mu$ M in the transition state.

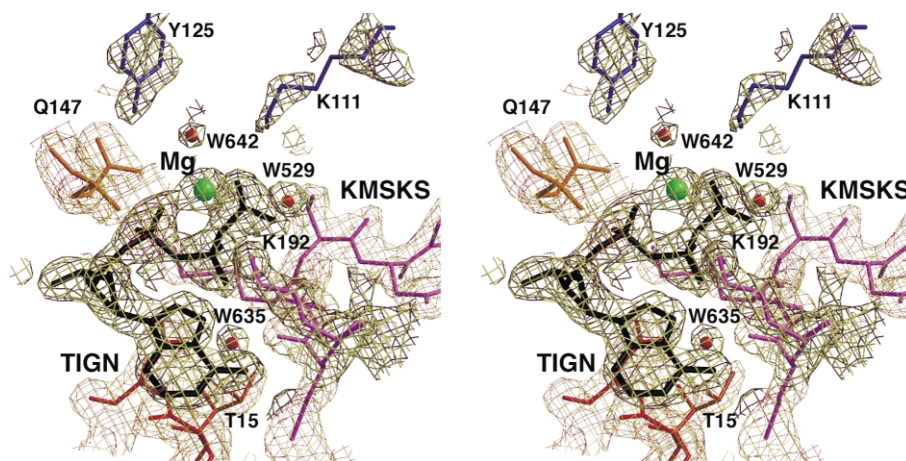


**Figure 11.** Final 2.2 Å electron density map contoured at 1.5 $\sigma$  showing the ATP-binding site in the closed, pre-TS conformation. The green ball corresponds to the model of the putative Mg<sup>2+</sup>.

hydrophobic selenomethionine may, however, change its binding characteristics, as the isomorphous residual map between SeMet and native crystals, using coefficients of the log-likelihood gradient computed by SHARP,<sup>39</sup> unexpectedly revealed a heart-shaped feature at 4 $\sigma$  in the indole pocket of the SeMet protein (Figure 13(b)). Features of this type of error synthesis usually are considered significant only above 6 $\sigma$ .

To assess the significance of this density for the closed, native TrpRS-ATP complex, we collected 2.2 Å data for the (isomorphous) abortive ternary complex formed with ATP and tryptophanamide in citrate pH = 7.5 buffer. Figure 13(c) shows both the  $\{|F_{\text{obs}}| - |F_{\text{calc}}|, \phi_{\text{refined,LF model}}\}$  map equivalent to that in Figure 13(a) and the  $\{|F_{\text{obs,TrpNH}_2\text{O}}| - |F_{\text{obs,ATP}}|, \phi_{\text{refined,LF model}}\}$  isomorphous difference map. Densities for the indole moiety are equally strong at 8 $\sigma$  in both difference maps, showing unambiguously that the indole pocket is empty in the binary ATP complex itself. Although a low

occupancy of the Trp-binding site by unidentified contaminants<sup>†</sup> in the SeMet derivative cannot be ruled out, the density in Figure 13(b) does not reflect occupation of the Trp-binding pocket of the native ATP complex.

<sup>†</sup> No indole group was added to the crystal growth medium (see Materials and Methods), thus neither the identification of the contaminant nor its occupancy in the crystal could be obtained with certainty. The most sensible source of contamination would seem to be variable amounts of adenine from degraded ATP. Its steric volume is comparable to that of indole and either the 6-amino group or a heterocyclic nitrogen could interact with the carboxylate group of D132 which recognizes the N<sup>e1</sup> nitrogen in indole. It would be surprising that a pocket sterically designed to discriminate between indole and phenol<sup>42</sup> could trap amounts of other compounds non-specifically, with high enough affinity to populate the site with near stoichiometric amounts of ligand.

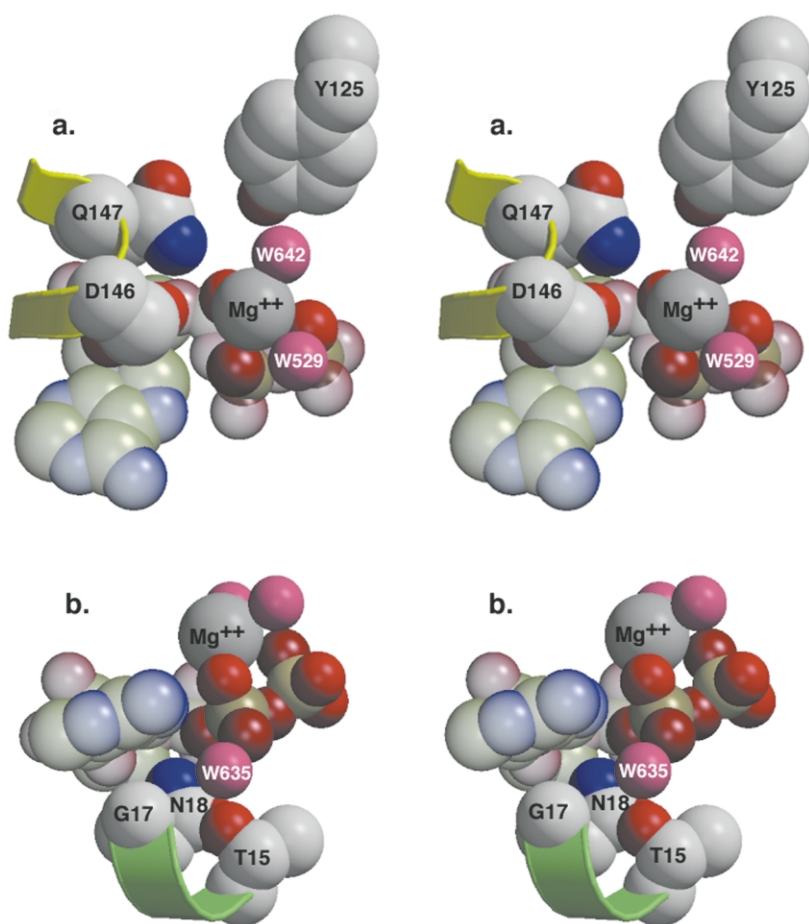


**Figure 12.** Polar interactions to the PP<sub>i</sub> leaving group. Water molecules are rose, non-bridging oxygen atoms red. (a) Deficient Mg<sup>2+</sup> coordination sphere. (b) Hydrogen bonding from the TIGN signature.

Crystallization trials have shown that monoclinic, not tetragonal, crystals grow from citrate solutions in the combined presence of ATP and tryptophan (P.R., unpublished results). Moreover, the significant shift of the F5 side-chain (by about 0.6 Å) into the cavity with respect to its position in all indole group complex structures (Figure 13(c)), is a clear indication of the absence of van der Waals interactions with a ligand. The near exact superimposability of the closed, pre-TS ATP complex and the abortive ternary complexes therefore demonstrates that ATP-binding interactions are both necessary and sufficient to assemble the TrpRS active site for catalysis.

#### ATP-induced rotation of Y125 closes the Trp-binding subsite

Despite the absence of Trp from the amino acid subsite, ATP binding induces coordinated rotations of Y125, Q107, and Q9 which narrow the mouth of the indole pocket in the closed ATP complex as observed in the adenylate product complex (Figure 9).<sup>4,14</sup> In open complexes, including the open Trp complex (Figure 5), the Y125 hydroxyl group is hydrogen-bonded to the carbonyl oxygen of Q105 and the imidazole of H150, preventing it from blocking access to the Trp-binding pocket even

after Trp binds. In most closed complexes, Y125 swings down to interact with the α-amino group, and in this orientation it blocks much of the remaining access to the tryptophan-binding subsite (Figure 8(a)). Thus, Y125 seems to serve as a gate, providing access to the ligand in the open ATP complex, and then properly aligning the α-carboxylate group with the α-phosphate *via* a hydrogen bond to the amino group after active-site assembly. We have difficulty placing this side-chain in the abortive tryptophanamide:ATP ternary complex, perhaps because it has the opportunity to bond either with the α-amino group or the α-amide group.

Y125 is conserved in class Ib and Ic aaRS<sup>6</sup> and is a key residue in α-amino group recognition. Its orientation here and in the adenylate product complexes of TrpRS and TyrRS is similar to that seen in the class Ia ArgRS:Arg complex,<sup>40</sup> in which the corresponding hydroxyl group also interacts with the α-nitrogen atom of the substrate. In contrast, the equivalent tyrosine in the class Ib GlnRS:tRNA complex, Y211,<sup>41</sup> specifically recognizes the side-chain amide nitrogen and not the α-amino group.

Elsewhere in the Trp subsite D132, a principal determinant for the indole group,<sup>42</sup> is unchanged compared to its position either in the Trp, adenylate, or IT complexes. Its carboxylate group is stabilized by H-bonds to imidazole nitrogens of

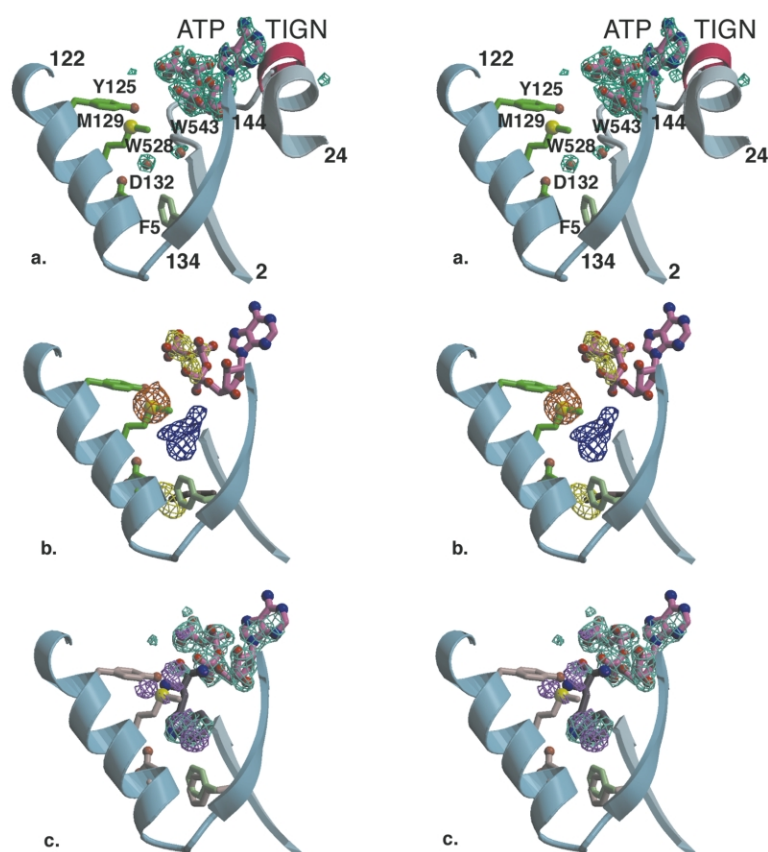


**Figure 13.** Difference Fourier maps related to the occupancy of the Trp-binding site. (a) The final  $\{|F_{\text{obs}}| - |F_{\text{calc}}|, \Phi_{\text{refined, unliganded model}}\}$  omit map. Side-chains surrounding the tryptophan-binding subsite and residue numbers for beginning and ending peptide segments are indicated. (b) Log-likelihood gradient difference map from SHARP (c)  $\{|F_{\text{obs, ATP}}| - |F_{\text{obs, ATP-TrpNH}_2\text{O}}|, \Phi_{\text{refined, unliganded model}}\}$  (magenta) and  $\{|F_{\text{obs}}| - |F_{\text{calc}}|, \Phi_{\text{refined, unliganded model}}\}$  (green) maps calculated for crystals grown with both ATP and tryptophanamide. All maps are contoured at  $4\sigma$ .

H86 and H43 (not shown), which are conserved in known TrpRS sequences, and by a water molecule, W528, in the closed ATP complex (Figure 9). Interactions with both histidines persist when the adenylyate is formed,<sup>4,14</sup> but are lost as a result of imidazole group rotation of H43 in the IT complex.<sup>13</sup>

### Structural evolution of the KMSKS loop and development of the $\text{PP}_i$ -binding subsite

Key changes are evident in the placement of the KMSKS loop in the closed complexes (Figures 14 and 15). The higher resolution of the present structures reveals an intensified hydrogen bonding and electrostatic interaction network that engages the oxygen atoms of the  $\text{PP}_i$ -leaving group, relative to the open ATP complex. In the latter complex, only the  $\alpha$ -amide nitrogens of K195 and S196, and the K192 side-chain from the KMSKS signature interact with the  $\text{PP}_i$  moiety. These interactions are retained in the pre-TS complex (Figure 14(b)). However, a subtle movement extends the KMSKS loop around the  $\text{PP}_i$ , bringing the  $\epsilon$ - $\text{NH}_3^+$  of lysine K195 and the OH group of S196 into contact with the  $\beta$  and  $\gamma$ -phosphates, respectively. Thus, three of the four negative charges borne by the triphosphate are compensated in the closed ATP complex by charged hydrogen bonds<sup>43</sup> to the side-chains of K192, K195, and of K111 which is recruited from across the domain boundary to interact with the

$\gamma$ -phosphate (Figure 13(b)). The remaining charge and that generated on the leaving group are doubtless compensated by the bound  $\text{Mg}^{2+}$  (Figure 12(a)).

Lysine K111 is positioned in close analogy with TyrRS residues K82 and R86,<sup>17,18</sup> which are missing in TrpRS. The average  $B$ -value of the loop to which it belongs,  $53.7 \text{ \AA}^2$ , suggests its flexibility. Deployment of this and the KMSKS loop around the  $\text{PP}_i$  leaving group from opposite sides of the active-site cleft is apparently homologous to the two elements of the induced-fit mechanism of Fersht.<sup>18</sup> Side-chains of two residues from the short belt, Q9 and S11, also target the  $\gamma$ -phosphate. S11 in TrpRS is homologous to T40 in TyrRS, whose distance from the reaction seat rendered its contribution to transition-state stabilization unexpected. Thus, the parallel between the TrpRS and TyrRS active-site configurations is even more extensive than previously recognized.<sup>4</sup>

The two polar side-chains from the TIGN signature form hydrogen bonds to the eventual  $\text{PP}_i$  leaving group (Figure 12(b)).  $\text{N}^{\delta 2}$  of N18 shares a bifurcated hydrogen bond between the  $\text{O}4'$  pyranose oxygen and the oxygen bridging  $\text{P}^\alpha$  and  $\text{P}^\beta$ . T15 is linked by hydrogen bonding through a bound water molecule (W506) to a non-bridging oxygen on  $\text{P}^\beta$  bringing new insight to the question of how the homologous mutations T15A in *E. coli* TrpRS and H45G, in *B. stearrowthermophilus* TyrRS destabilize their respective transition-states by  $2.3 \text{ kcal/mol}$ <sup>44</sup> and  $3.2 \text{ kcal/mol}$ ,<sup>45</sup> respectively,

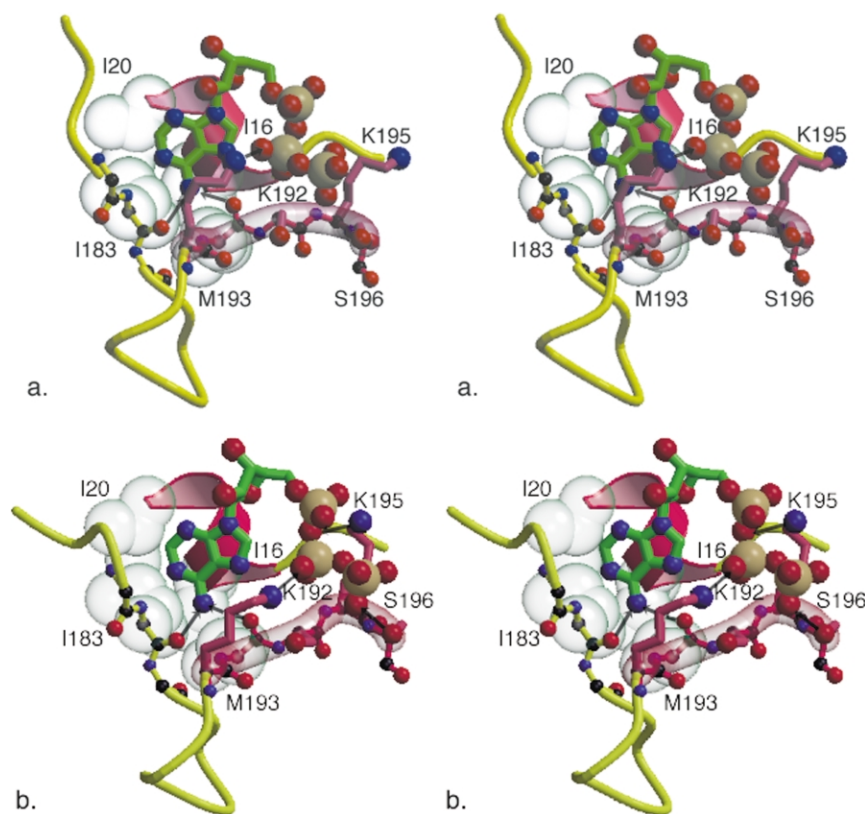


**Figure 14.** The PP<sub>i</sub>-binding subsite and development of interactions with the KMSKS signature (rose tube) through interaction with ATP in the pre-TS state. (a) Open ATP complex, in which the KMSKS loop is incompletely deployed such that K195 does not interact with the PP<sub>i</sub> moiety. (b) Complete deployment of the KMSKS loop incorporates both K195 and S196 into the pyrophosphate-binding site in the pre-TS ATP complex. Hydrogen-bonded interactions to adenosine and PP<sub>i</sub> moieties are reinforced by hydrophobic bonding between I183 and M193 from the long belt to I16 and I20 from the HIGH signature. The putative bound Mg<sup>2+</sup> is omitted.

with minimal loss in ATP affinity. This question could not be addressed on the basis of previous structures because both residues occupy positions too far from the  $\alpha$ -phosphate to make hydrogen-bonding contacts.

The TIGN and KMSKS signature residues interacting with the PP<sub>i</sub> are tied together and to the SD by van der Waals interactions involving I16, I20, I183, and M193 (Figure 14), enforcing the rigid body domain motion observed in TrpRS.<sup>10</sup> This non-polar cluster is reinforced by van der Waals contact between the T15 methyl group and the K195  $\alpha$ -carbon.

## Discussion

The open and closed TrpRS:ATP complexes demonstrate that titration of TrpRS with ATP produces two distinct, successive ATP-bound states, a result not observed in any previous aminoacyl tRNA synthetase structures. Interpretations are, of course, subject to the relevance of crystal structures to behavior in solution, of abortive complex structures to the actual reaction path, and of the structural cycle for a different, though closely related enzyme in the case of TyrRS studies. These considerations notwithstanding, the structures bring new structural perspective to several important questions first brought to light by the elegant mechanistic analysis by Fersht and co-workers of the TyrRS mechanism.<sup>18,19</sup> Structural

interpretation of those studies was limited, because there was only a single structure on which to base conclusions about results that strongly implied intramolecular motion.

The three families of TrpRS structures now complement the TyrRS mutational and kinetic studies in considerable detail, providing a novel basis for understanding the implications of Fersht's work. Our structural studies, confirmed here by ATP titrations monitored by SAXS and enzymatic activity that correlate the TrpRS crystal structures with solution behavior, establish the relevance of the conformational differences to the catalytic mechanism and shed important new light on the thermodynamics of the conformational equilibria.

The TrpRS:ATP interactions described here underscore Fersht's conclusion that ATP-binding free energy is used to drive active-site assembly in an induced-fit stage of the TyrRS-catalyzed reaction.<sup>15</sup> Further, the interactions that develop with ATP are so numerous and stereochemically optimal that they allow us to rephrase a second conclusion also drawn by Fersht, namely that the closed, pre-TS protein conformation is destabilized by the changes necessary to bind ATP in a catalytically productive mode.<sup>18</sup>

Our discussion will address first the order of binding, then the possible generality of our observations for other aaRS and, finally, the three questions posed at the outset and implications for free energy transduction.



essentially the same behavior: the dissociation constant for ATP from both E·ATP and E·Tyr·ATP complexes was found to be  $\sim 5$  mM, in close agreement with our TrpRS results. Those authors concluded, as we do, that the kinetically detected E·ATP complex was abortive and off-path. They could not attribute this behavior to specific structural properties, however, whilst the TrpRS structural data implicate premature closure of the active site as a likely explanation. The agreement between the behavior of the two enzymes on this crucial point is remarkable.

A third consideration posed by the order-of-binding question concerns the relevance of our closed E·ATP complex to Fersht's postulated high-energy complex formed between E·Tyr·ATP and E·Tyr·ATP\*. As noted below, the closed ATP complex is even weaker than the open complex. The closed ATP complex is structurally nearly identical with the ATP:tryptophanamide and other abortive ternary complexes. We believe that these complexes do indeed resemble the catalytically relevant pre-TS complex. More importantly, however, as described in the following, the ATP titrations permit more quantitative specification of just what makes this a "high-energy" complex.

### How general is the relative TrpRS domain motion?

Structures are now available for unliganded and ATP-complexed forms of *T. thermophilus* TyrRS,<sup>46</sup> the other class Ic aaRS, and for the two class Ib aaRS GluRS<sup>47</sup> and GlnRS (J. Perona, personal communication). TrpRS shows the most dramatic domain movement, but similar ligand-dependent conformational changes have been observed in each case. TyrRS studies are also in keeping with Fersht's earlier results. Structures from all three subclasses show similar redeployment of the KMSKS loop upon induced fit, moving the second lysine into contact with the  $\alpha$ -phosphate (S. Cusack *et al.*, unpublished results).<sup>46</sup> Unliganded and adenylate-inhibited structures of LeuRS<sup>48</sup> and of yeast ArgRS:Arg complex with and without cognate tRNA<sup>49</sup> suggest similar changes in class Ia synthetases. No comparable ATP-induced changes have yet been identified for any of the class II aaRS.

ATP binding to class Ib aaRS in the absence of cognate tRNA leads to complexes similar to the open TrpRS-ATP complex, without assembling the active-site interactions seen in the TrpRS closed, pre-TS state. Indeed, ATP and Glu bind simultaneously to GluRS such that the  $\alpha$ -carboxylate and  $\alpha$ -phosphate are almost exactly the same distance apart as they are in the corresponding singly-liganded TrpRS complexes.<sup>47</sup> These curious variations on the general theme provide a satisfying rationale for the long-recognized distinction that these three aaRS all require tRNA for amino acid activation. ATP binding to a fully assembled, catalytically competent active-site configuration is unfavorable enough in class Ib enzymes and in

ArgRS that cognate tRNA binding is required to overcome the forces resisting it.

Soaking an *Archaeon* class IIb AspRS<sup>50</sup> crystal revealed localized, ATP-induced reorientation of surface loops, similar in scale to those induced by amino acid binding. It is unclear how widespread these changes actually are in solution, because some of these changes have been observed after ligands were soaked into crystals of unliganded enzyme. When ligand-binding residues lie at a boundary between two domains, large domain rearrangement is expected and crystal packing may limit the extent of domain motion. Co-crystallization becomes the method of choice to get a particular liganded complex.

Full occupancy of the Trp-binding site is apparently incapable of closing TrpRS, as its configuration does not vary significantly from the open Trp complex to the final product state. Conformational consequences of Trp binding are evident only in the weak cooperativity with ATP (Figure 4(e)). Idiosyncratic variability in amino acid-induced conformational changes by different aaRSs suggests that most have some degree of amino acid-dependent conformational coupling. On binding methionine MetRS<sup>51</sup> undergoes a significant relative motion of the first and second halves of the RF. Amino acid binding to several class II aaRS structures caused loops to close around the substrate. Relative orientation changes between the N-terminal, anticodon-binding and C-terminal catalytic domains could be visualized after lysine binding to the class II LysRS.<sup>52</sup> Thus, the relative unimportance of Trp as an allosteric effector is curious.

### Binding interactions in the adenine nucleotide-binding subsites account for the dynamic TrpRS conformational cycle

When fully saturated by 10 mM ATP, the initial step of the TrpRS conformational cycle involved in catalysis, i.e. induced-fit assembly of the closed, pre-TS,<sup>13</sup> can be driven entirely by interactions with only one of the two reactants, the nucleotide triphosphate. The two distinct ATP complexes, solution scattering, and enzymological experiments described here implicate ATP as the predominant "allosteric" ligand. The structural separation of the two binding sites by  $\sim 7$  Å raises the question of what triggers the conformational change necessary to bring them together for amino acid activation. Interactions most likely to develop sufficiently to induce closure in saturating [ATP] are the numerous polar interactions with the ribose and PP<sub>i</sub>-binding subsites, (Figure 15). Closure around the triphosphate is favored by formation of 14 new hydrogen bonds, three of which involve charged groups and, therefore, should benefit from additional stability.<sup>43</sup> Thus, the conformational trigger probably lies in the intensification of electrostatic and hydrogen-bonded interactions with ATP from both halves of

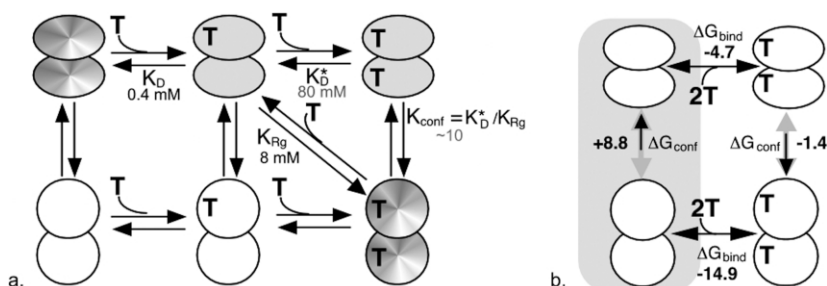


**Figure 16.** Linkage of TrpRS ATP (T) binding and conformational equilibria. (a) Estimation of the conformational equilibrium constant,  $K_{conf} \sim 10$  for converting the open, fully liganded TrpRS into the closed, pre-TS conformation, and the dissociation constant,  $K_d^* \sim 80 \text{ mM}$ , for the second ATP from the open TrpRS for the thermodynamic cycle in the upper right triangle.  $K_d$  is the dissociation constant for ATP

observed in [ATP] dependence of  $PP_i$  exchange.  $K_{Rg}$  refers to the ATP concentration estimated from SAXS measurements as necessary to induce closure as indicated by  $R_g$ . Crystal structures are known for open, unliganded and closed, fully liganded TrpRS (gradient) as well as for a state related to the singly and doubly liganded open conformation (shaded). (b) Free-energy differences in the TrpRS ligand-linked conformational cycle.  $\Delta G_{bind}$  values are estimated from the dissociation constants for ATP from TrpRS in  $PP_i$  exchange (open form), and that for GTP from Ras<sup>55</sup>(closed form).  $\Delta G_{conf}$  for fully liganded TrpRS is obtained from  $K_{conf}$ . In the absence of ligand, conformational energies strongly favor the open state of the enzyme. ATP-binding energy is used, in large part, to overcome the unfavorable Gibbs free energy required to assemble the active site for catalysis, as indicated by the shift in the direction of the conformational equilibrium. This energy cost significantly reduces the observed affinity of TrpRS for ATP and represents the storage of binding energy in the strained TrpRS conformation.

its bipartite-binding site. The high level of [ATP] required and the quadratic dependence (Figure 4(f)) implies that these interactions must develop in both subunits in order to overcome the energetic barrier to active site assembly in the absence of Trp.

### The catalytic role of the KMSKS loop

The new  $PP_i$ -binding interactions in Figure 15(b) result from two different structural changes. The domain movement itself recruits new interactions with Q9, S11, and K111, which are too distant in the open complex. In contrast, elongation of the KMSKS loop allows the K195 side-chain to curl around the triphosphate and find a nearly ideal electrostatic interaction with the  $\alpha$ -phosphate and brings the S196 OH group into hydrogen bonding distance with the  $\gamma$ -phosphate. The KMSKS loop thus becomes increasingly constrained in the process of active-site assembly. It also pulls M193 away from its location in the open complex (Figure 14(b)), “stretching” the hydrophobic core joining the two signatures to the SD. The [ATP]-dependence of the conformational change argues that formation of the fully developed KMSKS loop configuration (Figure 14(b)) also weakens the closed, pre-TS TrpRS:ATP affinity.

The subtle reconfiguration of the KMSKS loop recalls the fundamental observation of First & Fersht, that the TyrRS KFGKT variant disrupts an underlying synergy between ATP and tyrosine binding.<sup>7-9</sup> Deletion of the KFGKT loop in TyrRS paradoxically stabilizes ground-state Michaelis complex interactions with ATP, with a corresponding loss of differential affinity in the transition state. Thus, the stability of the ( $\Delta$ KFGKT)TyrRS:ATP complex increases with increasing tyrosine concentration, consistent with the positive cooperativity between Trp and [ATP] binding evident in the open conformation (Figure 4(e)), although to a

far greater extent. Synergistic coupling between the two binding sites also seems necessary for amino acid activation to proceed smoothly at ATP concentrations below the unphysiologically high<sup>53</sup> values required for induced-fit closure by ATP alone. Thus, domain movement must be more favorable when both substrates are bound than when only ATP is bound.

The TrpRS KMSKS loop therefore also probably disrupts an even stronger coupling between Trp and ATP binding expected from thermodynamic linkage. This conclusion deepens the similarity between TrpRS and TyrRS, and suggests a structural basis for the observations of First & Fersht: development of full binding by this loop (Figures 14(b) and 15(b)) comes at the expense of significant energetic cost to the protein, storing Gibbs free energy in the conformational change, which may be transferred to, and realized in, the transition state interaction.

The mechanistic relevance of the KMSKS loop, clarified by the structural data, is that by weakening the ground state interaction with ATP in the assembled active site, it helps avoid an off-path energetic “pit” in which both amino acid and ATP are tightly bound, impeding progress toward the transition state.<sup>9</sup>

### Weak ATP binding; half-site reactivity, and using ATP-binding energy for catalysis

The data presented here vividly confirm Fersht’s prescient description of what was, at the time, a hypothetical closed, pre-TS TyrRS configuration: “it is more likely that there is a high energy intermediate complex between E-Tyr-ATP and E-[Tyr-ATP]<sup>+</sup> in which the structure of the enzyme and interactions between it and the substrate resemble those of the transition state”.<sup>18</sup> Probably the most curious and far-reaching conclusion of

this work is the insight provided into the weak affinity of TrpRS and aaRS in general for ATP (Figure 16). The total surface area of ATP is  $629 \text{ \AA}^2$ , all but  $4 \text{ \AA}^2$  of which is buried from solvent access in the closed, pre-TS complex. Polar and electrostatic interactions in that complex appear to be nearly optimal (Figures 13–15). The ATP charges are neutralized and all hydrogen-bonding partners are satisfied, minimizing ATP's preference to remain in water. Yet, our SAXS measurements indicate that the [ATP] required, and hence the equilibrium constant for domain closure,  $K_{R_g} \sim 8 \text{ mM}$ , comparable to that required to grow tetragonal crystals.<sup>21</sup>

Thus, crystallization apparently does not significantly modulate the conformational equilibrium, and a modest excess of the closed form, perhaps tenfold, suffices to explain production of tetragonal crystals by mass action. Thus, the intrinsic conformational equilibrium constant for doubly liganded TrpRS,  $K_{\text{conf}} = K_{R_g}/K_d^* \sim 10$  ( $\Delta G \sim -1.4 \text{ kcal/mol}$ ). The thermodynamic cycle in Figure 16(a) therefore suggests that the binding of a second ATP molecule to a dimer containing one ATP is much less favorable than binding the first, and occurs with a  $K_d^* \sim 80 \text{ mM}$ , consistent with the half-site reactivity observed for TyrRS.<sup>29,30</sup>

The potential ATP binding affinity to the pre-TS conformation itself is clearly considerably higher. The rough proportionality between buried surface area and Gibbs free energy,  $25 \text{ cal/\AA}^2$ ,<sup>54</sup> suggests that forming the ATP complex described here might liberate  $\sim -15.6 \text{ kcal/mol}$ , and that the  $K_d$  should be  $\sim 5 \text{ pM}$ . This estimate is consistent, for example, with the affinity of Ras GTPase for GTP in the absence of exchange factors, which is  $\sim 17 \text{ pM}$ .<sup>55</sup> Thus, Ras exploits essentially all the potential binding determinants of the GTP, while the pre-TS TrpRS:ATP complex is some eight or nine orders of magnitude weaker.

We cannot identify any obvious deficiencies in the replacement of water molecules of hydration by hydrogen bonding to active-site functional groups (Figures 11 and 15), and conclude that the binding affinity of the closed, pre-TS form for ATP is close to that for the ras:GTP complex. Using that value, we calculate the conformational free energy for closing unliganded TrpRS to be  $\sim +8.8 \text{ kcal/mol}$  from the thermodynamic cycle in Figure 16(b). This value is comparable to the overall Gibbs energy released by ATP hydrolysis in water. The reduction in ATP-binding affinity from that which would potentially be available in a stably-configured optimal binding site, reflects the energetic cost of overcoming unfavorable protein structure changes necessary to form the pre-TS complex. We emphasize that in this sense, and much as was anticipated by Fersht,<sup>17</sup> Gibbs energy is "stored" in the destabilized or strained TrpRS conformation.

Ground-state destabilization is one of the canonical effects that can contribute to catalysis.<sup>56</sup> Too little is known about the actual transition state structure to determine the extent to which the

increased Gibbs energy of the TrpRS polypeptide component contributes to rate acceleration. However, it is unlikely that so significant a conformational effect could develop so close to the transition state structure without also influencing the catalytic rate. Fersht's work suggests two possibilities. The ground-state destabilization could be catalytic if binding the transition state for phosphoryl-transfer involves significant conformational rearrangement toward a conformation with lower Gibbs energy. The product state<sup>4,14</sup> may represent such a conformation. Alternately, the restabilized protein conformation in the product state may serve to retain the reactive adenylate intermediate until the cognate tRNA<sup>Trp</sup> can be provided to accept acyl transfer. Distinguishing between these possibilities requires a more precise structural description of the actual transition state.<sup>57–59</sup>

### What stabilizes the open conformation in the absence of two bound ATP molecules?

The balance of ATP-binding and conformational energies shifts the equilibrium conformation of the enzyme from open to closed, forcing the TrpRS:ATP complex to adopt an otherwise unfavorable conformation in order to realize additional binding interactions with ATP. Rearrangements of hydrophobic core packing interactions and their contribution to protein stability<sup>12</sup> are consistent with significant contributions to changes in overall conformational Gibbs energy and suggest that the closed, pre-TS state is the least stable conformation by a significant amount. These results will be discussed separately. Recent advances in computational biology now permit us to estimate conformational Gibbs energies from molecular dynamics simulations,<sup>60–63</sup> which are in progress.

### Induced-fit and catalysis

As detailed in Figure 15, there is extensive homology between interactions realized only in the TrpRS pre-TS structure and homologous amino acid residues in TyrRS whose binding affinity develops only in the transition state: D146 with the ribose and S11, Q9, K111, K195, and S196 to the PP<sub>i</sub>, include most or all of the residues homologous to those identified by Fersht's work as sources of differential, high transition-state affinity for ATP.<sup>17,18</sup> Moreover, the wholesale recruitment of new binding interactions to the ATP ribose and PP<sub>i</sub> moieties in the closed, pre-TS structure contrasts with the passive behavior of the Trp-binding subsite. The relative TrpRS domain motion and the meticulous preparation of ATP-binding interactions in this pre-TS ground state structure is thus a superb structural realization of the fundamental notions motivating the theory of induced-fit: a major geometric change occurs as the active site becomes ordered by the binding of substrate in order to set the stage for subsequent catalytic rearrangement in which the transition

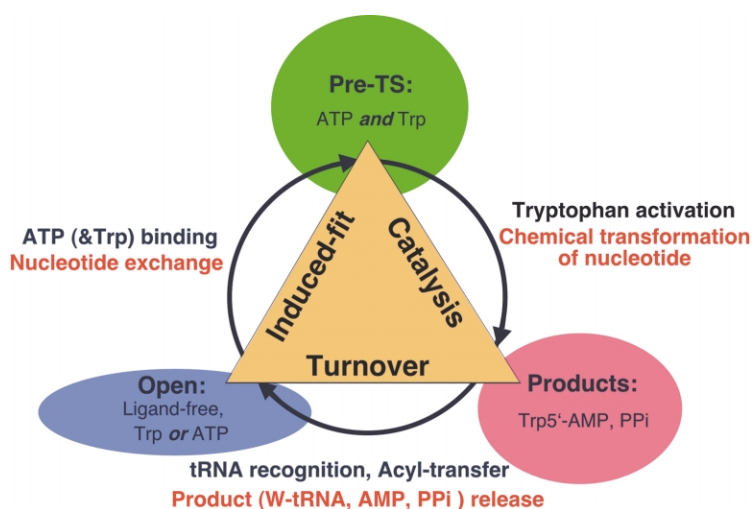


**Figure 17.** TrpRS three-state behavior and its homology to the conformational cycles of transducing enzymes. The three TrpRS conformational states are represented by open, closed, pre-TS and product complexes. Chemical and biochemical events associated with the conformational transitions between distinct states involved in ATP utilization are indicated outside the cycle, with TrpRS specific events in dark blue and their more generic biochemical descriptions in red. Conventional catalytic stages are indicated inside the triangle.

state itself becomes the target of additional interactions.<sup>64</sup>

The significance of the induced-fit theory for transfer reactions is reinforced by the paradoxically weak binding of ATP in the pre-TS state. Indeed, alignment of active-site residues has a dual role: first, to weaken the binding of substrate, which necessarily converts some binding energy into higher energy protein conformations; and second, to channel this stored conformational energy to other purposes. An important corollary of the specific structural realization of induced-fit in the TrpRS structures is that ATP binding and catalysis are somewhat independent events along the TrpRS reaction pathway, separated by the induced-fit active-site assembly.

The weak ATP affinity suggests that the binding interactions (Figures 12, 14–15) fall short of those yet to develop in the transition-state. Thus, the transition state itself likely differs from the ground-state configuration seen here, raising a new set of questions. If the nucleophilic attack is “associative” and catalyzed by moving the  $\alpha$ -phosphate toward the carboxylate group, the tryptophan being held in its invariant environment, then the structures lack an element considered essential for catalysis, namely high affinity for the pentavalent phosphoryl transition state.  $\text{PP}_i$  exchange is unaffected by vanadate and aluminium fluoride, inhibitors that mimic such a transition state.

On the other hand, a “dissociative” transition state, suggested by the significant relocation of the  $\text{PP}_i$  and its binding site in the products complexes, would benefit from effective strain on the  $\text{P}^\alpha\text{-P}^\beta$  bond. The subsequent conformational change observed in the product complex<sup>4,14</sup> suggests that effective strain might be exerted if the polypeptide destabilization in the pre-TS complex is restored in the product conformation. That mechanistic scenario would develop maximum binding affinity in the ribose and  $\text{PP}_i$  subsites as they move in opposite directions, favoring transient stretching

of the  $\alpha$ -phosphate- $\text{PP}_i$  bond to the leaving group. Such a mechanism would be consistent both with high level of transition state affinity and with the residue-by-residue reaction profile outlined by Fersht.<sup>17,18</sup>

#### ATP as an “allosteric effector” in transducing enzymes

The TrpRS:ATP system represents an extensively developed example of the widespread phenomenon of using linkage between conformational and ligand-binding equilibria<sup>65</sup> for free-energy transduction. Its three distinct structural states are strongly correlated with the nature of the productively bound adenine nucleotide ligand. The open state includes the Trp and sub-stoichiometric ATP complexes. The pre-TS state includes all of those complexes that develop what appear to be productive-binding interactions to the triphosphate. The product state invariably results when analogs of tryptophanyl-5' adenylylate are bound.

The hallmark of purine nucleoside triphosphatases (NTPases) is to couple a useful result to the NTPase cycle by differentiating the conformations of successive biochemical states and their intermolecular interactions, in accordance with the nucleotide ligand chemistry. The TrpRS behavior described by X-ray crystallography<sup>4,10,13,14</sup> and this work, is similar to the paradigm provided by the three different functional states of the multidomain S1 myosin head<sup>66</sup> and F1 ATPase<sup>67</sup> (Figure 17). A key point is that the magnitude of the Gibbs energy stored in TrpRS domain movements, 8–10 kcal/mol, is comparable to the large amounts transduced by similar, binding-change mechanisms during the synthesis and utilization of ATP by transducing assemblies,<sup>67</sup> as previously suggested.<sup>68</sup> The structural and functional homology between the three-state TrpRS cycle and those of transducing enzymes suggests to us that TrpRS, and perhaps more generally, class I aaRSs, belong to an NTPase superfamily.

## Materials and Methods

### Activity assays and active-site titration

PP<sub>i</sub> exchange rates were determined by a modification of the method described<sup>69</sup> in which 10 μl enzyme was added to 190 μl solutions containing 0.1 M Tris-HCl (pH 8.0), 10 mM KF, 5 mM MgCl<sub>2</sub>, 2 mM N<sub>4</sub>ATP, 2 mM Trp, 70 mM β mercaptoethanol; and 2 mM <sup>32</sup>P<sub>i</sub> at a specific radioactivity between 1 × 10<sup>5</sup> and 2 × 10<sup>5</sup> cpm/μM. Triplicate samples were incubated at 37 °C for 15 minutes, quenched with 2.5% perchloric acid on ice with the addition of 50 μl of 15% Norit A, and filtered onto Whatmann GF/C or GF/F filters, which were washed three times with 15 ml of deionized water and dried before scintillation counting. Michaelis-Menten experiments sampled Trp concentrations as in Table 2. Experiments varying Mg<sup>2+</sup> concentration used the same procedures, except that Mg<sup>2+</sup> concentrations were 1, 2, 3, 4, 5, 10, 15, 20, 30, 200, and 400 μM. Free Mg<sup>2+</sup> concentrations were estimated using the CHELATOR program.<sup>70</sup>

The concentration of competent TrpRS active sites was determined by active-site titration, essentially as described.<sup>27</sup> Reactions containing 5 μM <sup>32</sup>Pγ-ATP at a specific radioactivity of ~5000 cpm/pM; 10 mM MgCl<sub>2</sub>; 0.14 M Tris-HCl (pH 7.8), 1 mM Trp, 1–2 μM TrpRS and 2 units/ml pyrophosphatase were incubated at 25 °C. Triplicate 20 μl aliquots were withdrawn at intervals, quenched with 100 μl 7% perchloric acid, extracted with 200 μl 2% Norit A, and filtered and washed as described above. The number of active sites was determined by extrapolation of the linear portion of the decay to zero time value, which was determined before adding enzyme.

Values obtained were used to evaluate *k*<sub>cat</sub> for native and SeMet TrpRS from Michaelis-Menten experiments performed with the titrated enzyme. Substitution of selenomethionine for methionine increased the second order rate constant by twofold, which resulted from an increase in both *K*<sub>m</sub> (from 2 μM to 4 μM) and *k*<sub>cat</sub> (from 11 s<sup>-1</sup> to 43 s<sup>-1</sup>).

### Small angle X-ray scattering

Solution scattering experiments involved joint, full-factorial variation of pH, TrpRS (4 mg/ml and 8 mg/ml), Trp (0 mM and 0.2 mM), and ATP (0 mM and 10 mM) concentrations according to a design matrix similar to that described,<sup>21</sup> except that the temperature was kept constant (ca 21 °C) while the enzyme concentration was varied. In this way, 16 different experimental conditions were explored. All samples were equilibrated against 0.8 M K<sub>2</sub>PO<sub>4</sub> at the appropriate pH. Scattering curves were recorded on the SAXS instrument D24 using synchrotron radiation emitted by a bending magnet on the storage ring DCI at LURE (Orsay, France). The instrument, data acquisition system<sup>71</sup> and evacuated measuring cell<sup>72</sup> have been described. Data were recorded over the angular range 0.0016 Å<sup>-1</sup> < *s* < 0.022 Å<sup>-1</sup>, where *s* = (2 sin θ)/λ is the modulus of the scattering vector, 2θ is the scattering angle, λ (1.49 Å) is the radiation wavelength. Eight frames of 100 s or 200 s each were recorded depending on sample concentration. Frames were visually inspected to check for X-ray damage; none was found. All data were scaled to the transmitted intensity, before computing the average and standard deviation of each

measurement and subtracting the scattering from the corresponding buffer.

At very small angles, the intensity scattered by a particle can be approximated by a Gaussian curve:<sup>73</sup>

$$I(s) = I(0) \exp(-4\pi^2 s^2 R_g^2 / 3)$$

and the slope of a Guinier plot (ln[I(*s*)] versus *s*<sup>2</sup>) readily yields *R*<sub>g</sub> for the particle. This approximation is valid over a restricted *s*-range (typically 2π*R*<sub>g</sub>*s* < 1.3). For each investigated condition, the value of the radius of gyration was derived on multiple replicates from a Guinier analysis performed over the appropriate *s*-range.

Statistical modeling was carried out using SYSTAT<sup>74</sup> and JMP<sup>75</sup> using stepwise regression to evaluate a range of models, and standard least-squares regression to evaluate the best model. pH values of all samples were determined following the measurements, and did not in all cases correspond to those intended in the original design, owing in part to the unexpected importance of the ATP. Values were grouped into three obvious clusters for the purpose of plotting in Figure 3.

### Crystallization

*B. stearothermophilus* native and selenomethionyl TrpRS were purified as described.<sup>76</sup> All complexes were crystallized by microdialysis (5 μl of ~4 mg/ml protein versus a 2 ml well). Monoclinic crystals of the open Trp and ATP complexes were grown at 42 °C and pH 6.6 in a potassium phosphate buffer (2 M) either in the presence of 2 mM Trp or 1 mM (freshly dissolved and titrated) ATP (SIGMA) 20 mM MgCl<sub>2</sub>. All tetragonal crystals were grown at 35 °C. The protein stock buffer (0.6 M potassium phosphate solution in the presence of 50% (v/v) glycerol) was extensively exchanged by a precipitant solution containing ~1 M sodium citrate, 10 mM (freshly dissolved) ATP (SIGMA), and 10 mM MgCl<sub>2</sub>·50 μM TrpNH<sub>2</sub>O (tryptophanamide) was added with ATP for comparison with previous ATP:Trp analog complex crystals grown in potassium phosphate (X.H., unpublished results). Tetragonal ATP complex crystals were, however, hard to reproduce in phosphate, and we had difficulty characterizing them. Reproducibility was ultimately achieved by using citrate, rather than phosphate, as the crystallizing anion. Data collection provided quite good statistics compared to data from similar crystal forms obtained in phosphate Table 3. Trp was rigorously excluded from these crystal growth experiments.

Crystals grew within a week without further additives. Monoclinic crystals of the open complexes were collected at room temperature. Tetragonal crystals were quickly dipped into a 15% glycerol cryoprotectant solution prior to flash cooling in the 100 K-nitrogen stream. Cryopreservation extended diffraction to higher resolution limits (<2.2 Å for the native, 2.3 Å for the Se-derivative) compared to 2.5 Å (2.8 Å) at room-temperature. Mosaicity increased slightly (0.45° versus 0.3°). Another SeMet complex crystal dataset also collected to the same resolution limit on the RAXIS IV. Mosaicity for the ternary complex refined to 0.75° in spite of one annealing step.

### Structure solution and refinement

Data were integrated by DENZO and scaled independently using SCALEPACK,<sup>77,78</sup> Table 4, reduced using TRUNCATE,<sup>79</sup> and scaled to each other between 8 Å

**Table 4.** Data reduction for native TrpRS and selenium derivative and phasing statistics

	Native, open Trp complex	Native, open ATP complex	Native, "closed" ATP complex	Native, closed ATP + TrpNH <sub>2</sub> O	SeMet, closed ATP complex
Unit cell	C2 $a = 228.73 \text{ \AA}$ , $b = 92.24 \text{ \AA}$ , $c = 157.59 \text{ \AA}$ , $\beta = 132.71^\circ$	C2 $a = 228.55 \text{ \AA}$ , $b = 91.98 \text{ \AA}$ , $c = 156.89 \text{ \AA}$ , $\beta = 132.34^\circ$	$P4_32_12$ $a = b = 62.13 \text{ \AA}$ , $c = 217.81 \text{ \AA}$	$P4_32_12$ $a = b = 61.68 \text{ \AA}$ , $c = 218.78 \text{ \AA}$	$P4_32_12$ $a = b = 61.95 \text{ \AA}$ , $c = 217.91 \text{ \AA}$
No. of measured reflections	120,955	102,635	303,099	335,452	366,741
No. of unique reflections	55,705	42,607	24,329	23,318	30,265*
Resolution limits (Å)	2.7	3	45–2.15	25–2.10	25–2.3
Completeness (%)					
Overall	83.1	87.3	97.5 (up to 2.40 Å)		99.0 (up to 2.60 Å)
Last bin	50.4 (2.7–2.8 Å)	70.5 (3.11–3.0 Å)	12.1 (2.23–2.15 Å)	77.5 (2.18–2.10 Å)	38.0 (2.38–2.30 Å)
Reflections with $I > 3\sigma(I)$ (%)	–	–	82.3	76	82.1
Overall $R_{\text{sym}}$	0.079	0.079	0.08	0.079	0.08
$R_{\text{sym}}$ for last bin			0.31 (2.23–2.15 Å)	0.32 (2.18–2.10 Å)	0.30 (2.38–2.30 Å)
⟨Redundancy⟩	–	–	8.2	5.5	7.1*
Dataset	–	–	1	2	3
SIR phasing to 2.3 Å	–	–	1–3	2–3	3–1
Number of sites per molecule	–	–	Ten Se–S	Nine Se–S	Ten SeMet/328 res
$R_{\text{iso}}$ (%) data between 8 Å and 4 Å	–	–	0.125	0.198	
Phasing power (cent/acent)	–	–	1.8/2.4	1.0/1.2	1.7/2.0
$R_{\text{cullis}}$ (cent/acent)	–	–	0.61/0.62	0.87/0.88	0.61/0.63
FOM					
Cent/acent	–	–	0.461/0.379	0.24/0.22	0.35/0.37
After SOL-OMON	–	–	0.808	0.810	
Averaged phase difference to refined model					
SHARP SIR/SOL-OMON	–	–	60.4°/29.7°	70.4°/42.3°	63.9°/30.4°
Centroid phases/ $\sigma_A$	–	–	6.6°/25.7°	6.7°/27.3°	6.0°/26.1°

The  $R_{\text{sym}}$  is defined as:

$$\frac{\sum_{h,k,l} \sum_i |I(h,k,l) - \langle I(h,k,l) \rangle|}{\sum_{h,k,l} \sum_i I(h,k,l)}$$

where  $I_i(h,k,l)$  is the  $i$ th observation of reflection  $h, k, l$  and  $\langle I(h,k,l) \rangle$  is the weighted mean of all observations (after rejection of outliers). The  $R_{\text{iso}}$  is defined as:

$$R_{\text{iso}} = \frac{\sum_{h,k,l} |F_{\text{der}} - F_{\text{nat}}|}{\sum_{h,k,l} F_{\text{nat}}}$$

where  $F_{\text{nat}}$  and  $F_{\text{der}}$  are the native and derivative structure factor amplitudes, respectively. The phasing power is  $P_{\text{power}} = \langle |F_{\text{nat}}(\text{calc})| / \text{phase-integrated lack of closure} \rangle$ . The  $R_{\text{cullis}}$  is  $R_{\text{cullis}} = \langle \text{phase-integrated lack of closure} \rangle / \langle |F_{\text{der}} - F_{\text{nat}}| \rangle$ .

\* Friedel pairs are kept separated.

and 4 Å with SCALEIT,<sup>80,81</sup> native [10 mM ATP] data being taken as reference. Open complexes with Trp and ATP are isomorphous to LF crystals, and the three independent dimers in the asymmetric unit were refined directly using initial phase sets derived from that structure.<sup>10</sup> For the closed ATP complex, molecular replacement was performed to determine initial phases for the subset of Se–S atoms using AMoRe<sup>82</sup> in order to start heavy-atom parameter refinement using SHARP<sup>39</sup> for SIR phasing. Three known conformations for TrpRS

monomer (LF (id code: 1D2R), IT complex,<sup>13</sup> and adenylylate product complex (id code: 1I6M)) were tested as search models, after removing ligand and solvent molecules. The cross-rotation function was calculated between 8 Å and 4 Å resolution. The highest peak of the rotation function was subjected to a translation function search and then rigid-body fitting.

Positions, occupancies, and isotropic and anisotropic temperature factors for the ten heavy-atom sites were refined appropriately for an Se–S SIR experiment, by

**Table 5.** Results of structure refinement

	Native, open Trp	Native, open ATP	Native, closed ATP	Native, closed ATP + TrpNH <sub>2</sub> O	SeMet, closed ATP
No. reflections (all)	58,869	42,607	20,306	24,050	19,286
No. reflections (used for refinement)	49,817	38,186	17,449	19,973	15,680
No. reflections (used for <i>R</i> -free)	5594	4285	1986	2254	1789
No. protein atoms	15,468	15,392	2623	2605	2583
No. solvent atoms (water)	0	0	187(168)	152(119)	178(143)
No. ligand atoms	90	186	31	31/15	31
Averaged <i>B</i> -value for protein atoms (Å <sup>2</sup> )	46.8	37.4	25.6	35.4	22
Averaged <i>B</i> -value for solvent atoms (Å <sup>2</sup> )	–	–	30.9	42.8	29
Averaged <i>B</i> -value for ligand atoms (Å <sup>2</sup> )	24.2	59.5	21.5	27.9/38.4	19.8
Range of spacings (Å)	15–2.7	15–3.0	20–2.2	20–2.15	20–2.35
<i>R</i> -value (work) (%)	17.3	15.4	21	20.9	19.6
<i>R</i> -free (10% reserved) (%)	24.3	23.9	25.2	24.4	24
Ramachandran diagram (core/allow-gener/disall)	87.8/11 1.1/0	86.8/11.1 1.5/0	95.5/4.5 0/0	95.9/3.8 0.3/0	94.8/4.8 0.3/0
Weighted rmsd from ideality					
Bond length (Å)	0.009	0.012	0.006	0.006	0.006
Bond angle (deg.)	1.02	1.36	0.986	0.975	1.013

The crystallographic *R*-factor is defined by  $\sum |F_{\text{obs}}| - |F_{\text{calc}}| / \sum |F_{\text{obs}}|$  and indicates the accuracy of the model. The free *R*-factor is a cross validation residual calculated using 10% of the native data which were randomly chosen and excluded from the refinement.

SHARP. The weak anomalous signal was treated by SHARP, introducing the refinement of Se–S scattering factors. Initial values for  $f'$  and  $f''$  for Cu K $\alpha$  were estimated,<sup>83</sup> after subtracting the contribution of sulfur atoms from the selenium atoms. SIR phases for ten selenomethionines (from a total of 328 residues)<sup>84</sup> reduced bias from the initial molecular replacement model. A second SeMet TrpRS:ATP and ATP:tryptophanamide complexes were solved subsequently by molecular replacement. Note that anomalous residual maps using coefficients of the log-likelihood gradient function were able to locate sulfur atoms (peaks > 4 $\sigma$ ) from all methionine residues and three cysteines, C35, C38, and C95, and also  $\alpha$  and  $\beta$ -phosphorus atoms (Figure 13(b)).

SOLOMON as implemented in SHARP<sup>81,85</sup> was performed with a flipping factor of –1 for 130 cycles, during which the solvent sphere radius was reduced from 2.4 Å to the maximum resolution of the data. The disordered solvent content was estimated at 47% by maximizing the correlation coefficient on  $E^2$  from SIGMAA.<sup>86</sup> Electron-density maps were calculated with FFT and MAPMASK<sup>81</sup> and displayed in the program O<sup>87</sup> via the interface with SHARP.

The open Trp complex was refined using CNS.<sup>88</sup> Other structure solutions, including the open monoclinic ATP complex, were refined using BUSTER, developed by GlobalPhasing, Ltd and interfaced with TNT.<sup>89</sup> Bulk solvent and the random distribution of missing atoms were kept fixed. By keeping an appropriate distance from the data, maximum-likelihood methods limit over-fitting the observed amplitudes at phases too close to those of the initial fragment, which leads to the model bias to which least-squares is vulnerable. The truncated pieces are utilized as model-based non-uniform prior to output low-resolution distributions and together with the bulk solvent envelope and the fragment model, will account for the real-space picture of the crystal content. Maximum-entropy modulation of the envelope for missing atoms aims at recovering accurate density in their expected regions.<sup>90</sup> The refined atomic models comprised 2599 protein atoms from residues 1 to 326, not including the last two C-terminal arginine residues, which never have been observed in any TrpRS structures, and variable numbers of solvent molecules (Table 5). PDB ID

codes: Open Trp complex, 1MB2; Open ATP complex, 1MAW; Closed, pre\_TS ATP complex, 1M83; Closed, pre-TS tryptophanamide:ATP complex, 1MAU.

### Solvent and counter ion structure

The 2.2 Å crystallographic data and SIR experimental phases allowed us to position 171 water molecules in the electron density of the ATP complex, contrasting with the solvent-free 2.9 Å IT pre-TS structure (Y.Y. *et al.*, unpublished results). Additionally, three cryoprotective glycerol molecules were located, one of which occupies a similar position to that observed in the TAM complex nearby a cationic site close to the N-terminal region of the RF, evidenced previously in the 1.7 Å structure of the latter complex.<sup>14</sup> A second glycerol is located at the entrance of the active site cleft, near the  $\gamma$ -phosphate, making two H-bonds with O2 of Q49 and the S11 carbonyl oxygen atom. The third glycerol is located on the surface of the SD, interacting with  $\epsilon$ -NH<sub>3</sub> of K218, O<sup>71</sup> of T222 and  $\epsilon$ -NH<sub>3</sub> of K269, where a sulphate ion was found in the TAM complex.<sup>14</sup>

No specific citrate ion positions could be derived, although some solvent regions remained noisy at this resolution. Thus, we can suggest no role for citrate in stabilizing the ATP complex for crystallization. It is noteworthy for the second selenomethionylated complex and also the ATP:tryptophanamide complex that a sodium cation might fit within an octahedral environment of a cationic-binding site evident in several recent TrpRS product complex crystal structures.<sup>14</sup> Particularly short coordination distances (<2.5 Å), high *B*-factors with respect to the environment (>50 Å<sup>2</sup> or about twice those of surrounding carbonyls) and the absence of density for the other 10 mM ATP structures render the cationic identity dubious. The ambiguous occupancy of this site by sodium could be lifted by soaking this crystal in rubidium-containing solutions.<sup>91</sup>

### Superposition for structure analysis

For coordinate comparisons, models were superimposed using 42 C $^{\alpha}$  atoms taken from the first half of

the RF domain, which has been used as a reference orientation for previous comparisons among class I aaRSs.<sup>4</sup> Other comparisons involved superimposing the adenine moieties of different ATP complexes. Superpositions were performed using CDSFIT.<sup>81</sup>

## Acknowledgements

This work was supported by NIGMS-48519. We are grateful also to LURE for support during the SAXS measurements and to Globalphasing Ltd for licenses for SHARP and BUSTER/TNT and for their assistance. M. Ries-Kautt provided valuable advice during the SAS measurements. We gratefully acknowledge substantive discussions with J. Hermans, E. First, S. Cusack, and W. W. Cleland, which clarified several important issues addressed in this paper. T. Traut, M. Caplow, L. S. Kaguni provided helpful feedback on the manuscript. We are also grateful to S. Cusack, S. Yokoyama, J. Perona, and J. LaPointe for sharing information about structures of unliganded T. thermophilus TyrRS, GlnRS, and GluRS and various of their complexes before publication. Molecular graphics were prepared using MOLSCRIPT<sup>92</sup> and BOBSCRIPT,<sup>93</sup> and rendered with RASTER3D.<sup>94</sup>

## References

- Carter, C. W., Jr (1993). Cognition, mechanism, and evolutionary relationships in aminoacyl-tRNA synthetases. *Annu. Rev. Biochem.* **62**, 715–748.
- Schimmel, P., Giegé, R., Moras, D. & Yokoyama, S. (1993). An operational RNA code for amino acids and possible relationship to genetic code. *Proc. Natl Acad. Sci. USA*, **90**, 8763–8768.
- Xin, Y., Li, W., Dwyer, D. S. & First, E. A. (2000). Correlating amino acid conservation with function in tyrosyl-tRNA synthetase. *J. Mol. Biol.* **303**, 287–298.
- Doublé, S., Bricogne, G., Gilmore, C. J. & Carter, C. W., Jr (1995). Tryptophanyl-tRNA synthetase crystal structure reveals an unexpected homology to tyrosyl-tRNA synthetase. *Structure*, **3**, 17–31.
- Moras, D. (1992). Aminoacyl-tRNA synthetases. *Curr. Opin. Struct. Biol.* **2**, 138.
- Landès, C., Perona, J. J., Brunie, S., Rould, M. A., Zelwer, C., Steitz, T. A. & Risler, J. L. (1995). A structure-based multiple sequence alignment of all class I aminoacyl-tRNA synthetases. *Biochimie*, **77**, 194–203.
- First, E. A. & Fersht, A. R. (1993). Mutation of lysine 233 to alanine introduces positive cooperativity into tyrosyl-tRNA synthetase. *Biochemistry*, **32**, 13651–13657.
- First, E. A. & Fersht, A. R. (1993). Mutational and kinetic analysis of a mobile loop in tyrosyl-tRNA synthetase. *Biochemistry*, **32**, 13658–13663.
- First, E. A. & Fersht, A. R. (1995). Analysis of the role of the KMSKS loop in the catalytic mechanism of the tyrosyl-tRNA synthetase using multmutant cycles. *Biochemistry*, **34**, 5030–5043.
- Ilyin, V. A., Temple, B., Hu, M., Li, G., Yin, Y., Vachette, P. & Carter, C. W., Jr (2000). 2.9 Å crystal structure of ligand-free tryptophanyl-tRNA synthetase: domain movements fragment the adenine nucleotide binding site. *Protein Sci.* **9**, 218–231.
- Carter, C. W., Jr, Ilyin, V. A., Huang, X., Yin, Y., Hu, M., Longo, A. & Retailleau, P. (1999). *IUCr International Congress*, Glasgow, Scotland.
- Carter, C. W., Jr, Ilyin, V. A., Yin, Y., Huang, X. & Retailleau, P. (2002). *Using Crystallography to Understand Enzyme Mechanism*, St. Paul, MN.
- Yin, Y. (1995). *Crystallographic Study of Bacillus stearothermophilus Tryptophanyl-tRNA Synthetase in the Catalytic Reaction*. PhD, University of North Carolina at Chapel Hill.
- Retailleau, P., Hu, M., Bricogne, G., Vornrhein, C., Roversi, P., Blanc, E., Sweet, R. M. & Carter, C. W., Jr (2001). High resolution experimental phases for tryptophanyl-tRNA synthetase (TrpRS) complexed with tryptophanyl-5'AMP. *Acta Crystallog. sect. D*, **57**, 1595–1608.
- Fersht, A. R., Leatherbarrow, R. J. & Wells, T. N. C. (1986). Binding energy and catalysis: a lesson from protein engineering of the tyrosyl-tRNA synthetase. *Trends Biochem. Sci.* **11**, 321–325.
- Fersht, A. R., Leatherbarrow, R. J. & Wells, T. N. C. (1987). Structure–activity relationships in engineered proteins: analysis of use of binding energy by linear free energy relationships. *Biochemistry*, **26**, 6030–6038.
- Fersht, A. R. (1987). Dissection of the structure and activity of the tyrosyl-tRNA synthetase by site-directed mutagenesis. *Biochemistry*, **26**, 8031–8037.
- Fersht, A. R., Knill Jones, J. W., Bedouelle, H. & Winter, G. (1988). Reconstruction by site-directed mutagenesis of the transition state for the activation of tyrosine by the tyrosyl-tRNA synthetase: a mobile loop envelopes the transition state in an induced-fit mechanism. *Biochemistry*, **27**, 1581–1587.
- Fersht, A. (1988). Dissection of the structure and activity of an enzyme. In *Design of Enzymes and Enzyme Models* (Kaiser, E. T., ed.), vol. XXXI, pp. 159–182, Robert A. Welch Foundation, Houston, TX.
- Carter, C. W., Jr & Carter, C. W. (1979). Protein crystallization using incomplete factorial experiments. *J. Biol. Chem.* **254**, 12219–12223.
- Carter, C. W., Jr, Doublé, S. & Coleman, D. E. (1994). Quantitative analysis of crystal growth: tryptophanyl-tRNA synthetase polymorphism and its relationship to catalysis. *J. Mol. Biol.* **238**, 346–365.
- Carter, C. W., Jr & Yin, Y. (1994). Quantitative analysis in the characterization and optimization of protein crystal growth. *Acta Crystallog. sect. D*, **50**, 572–590.
- Piszkiwicz, D. (1977). *Kinetics of Chemical and Enzyme-catalyzed Reactions*, Oxford University Press, New York.
- Box, G. E. P., Hunter, W. G. & Hunter, J. S. (1978). *Statistics for Experimenters*, Wiley Interscience, New York.
- Wells, T. N. C., Knill-Jones, J. W., Gray, T. E. & Fersht, A. R. (1991). Kinetic and thermodynamic properties of wild-type and engineered mutants of tyrosyl-tRNA synthetase analyzed by pyrophosphate exchange kinetics. *Biochemistry*, **30**, 5151–5156.
- Joseph, D. R. & Muench, K. (1971). Tryptophanyl-transfer ribonucleic acid synthetase of *Escherichia coli* II. Molecular weight, subunit structure, sulfhydryl content, and substrate-binding properties. *J. Biol. Chem.* **246**, 7610–7615.
- Fersht, A. R., Ashford, J. S., Bruton, C. J., Jakes, R., Koch, G. L. E. & Hartley, B. S. (1975). Active site

- titration and aminoacyl adenylate binding stoichiometry of aminoacyl-tRNA synthetases. *Biochemistry*, **14**, 1–4.
28. Coleman, D. E. & Carter, C. W., Jr (1984). Crystals of *Bacillus stearotherophilus* tryptophanyl-tRNA synthetase containing enzymatically formed acyl transfer product tryptophanyl-ATP, an active site marker for the 3' CCA terminus of tryptophanyl-tRNA<sup>Trp</sup>. *Biochemistry*, **23**, 381–385.
  29. Ward, W. H. & Fersht, A. R. (1988). Asymmetry of tyrosyl-tRNA synthetase in solution. *Biochemistry*, **27**, 1041–1049.
  30. Ward, W. H. & Fersht, A. R. (1988). Tyrosyl-tRNA synthetase acts as an asymmetric dimer in charging tRNA. A rationale for half-of-the-sites activity. *Biochemistry*, **27**, 5525–5530.
  31. Fersht, A. R., Mulvey, R. S. & Koch, G. L. (1975). Ligand binding and enzymic catalysis coupled through subunits in tyrosyl-tRNA synthetase. *Biochemistry*, **14**, 13–18.
  32. Hogue, C. W. V., Doublé, S., Xue, H., Wong, J., Carter, C. W., Jr & Szabo, A. G. (1996). A concerted, tryptophanyl-adenylate dependent conformational change in *B. subtilis* tryptophanyl-tRNA synthetase revealed by the fluorescence of tryptophan 92. *J. Mol. Biol.* **260**, 446–466.
  33. Sever, S., Rogers, K., Rogers, M. J., Carter, C. W., Jr & Söll, D. (1996). *E. coli* tryptophanyl-tRNA synthetase mutants selected for tryptophan auxotrophy implicate the dimer interface in optimizing amino acid binding. *Biochemistry*, **35**, 32–40.
  34. Jahn, M., Rogers, M. J. & Söll, D. (1991). Anticodon and acceptor stem nucleotides in tRNA<sup>Gln</sup> are major recognition elements for *E. coli* glutamyl-tRNA synthetase. *Nature*, **352**, 258–260.
  35. Rogers, M. J., Adachi, T., Inokuchi, H. & Söll, D. (1992). Switching tRNA<sup>Gln</sup> identity from glutamine to tryptophan. *Proc. Natl Acad. Sci. USA*, **89**, 3463–3467.
  36. Schramm, V. L. & Wedler, F. C. (1986). *Manganese in Metabolism and Enzyme Function* (Press, A., ed.), New York.
  37. Bock, C. W., Kaufman Katz, A., Markham, G. D. & Glusker, J. P. (1999). Manganese as replacement for magnesium and zinc: functional comparison of the divalent ions. *J. Am. Chem. Soc.* **121**, 7360–7372.
  38. Beese, L. & Steitz, T. A. (1991). Structural basis for the 3'-5' exonuclease activity of *Escherichia coli* DNA polymerase I: a two metal ion mechanism. *EMBO J.* **10**, 25–33.
  39. de La Fortelle, E. & Bricogne, G. (1997). Maximum-likelihood heavy-atom parameter refinement for multiple isomorphous replacement and multiwavelength anomalous diffraction methods. *Methods Enzymol.* **276**, 472–494.
  40. Cavarelli, J., Delagoutte, B., Eriani, G., Gangloff, J. & Moras, D. (1998). L-Arginine recognition by yeast arginyl-tRNA synthetase. *EMBO J.* **18**, 5438–5448.
  41. Rath, V., Sylvian, L., Beijer, B., Sproat, B. S. & Steitz, T. A. (1998). How glutamyl-tRNA synthetase selects glutamine. *Structure*, **6**, 439–449.
  42. Praetorius-Ibba, M., Stange-Thomann, N., Kitabatake, M., Ali, K., Soll, I., Carter, C. W., Jr, Ibba, M. & Soll, D. (2000). Ancient adaptation of the active site of tryptophanyl-tRNA synthetase for tryptophan binding. *Biochemistry*, **39**, 13136–13143.
  43. Fersht, A. R., Shi, J.-P., Knill-Jones, J., Lowe, D. M., Wilkinson, A. J., Blow, D. M., Brick, P., Carter, P., Waye, M. M. Y. & Winter, G. (1985). Hydrogen bonding and biological specificity analysed by protein engineering. *Nature*, **314**, 235–238.
  44. Chan, K. W. & Koeppe, R. E. n. (1994). Role of the TIGN sequence in *E. coli* tryptophanyl-tRNA synthetase. *Biochim. Biophys. Acta*, **1205**, 223–229.
  45. Fersht, A. R., Leatherbarrow, R. J. & Wells, T. N. C. (1986). Structure and activity of the tyrosyl-tRNA synthetase: the hydrogen bond in catalysis and specificity. *Philos. Trans. R. Soc. Lond.* **317**, 305–320.
  46. Yaremchuk, A., Kriklivyi, I., Tukalo, M. & Cusack, S. (2002). Class I tyrosyl-tRNA synthetase has a class II mode of cognate tRNA recognition. *EMBO J.* **21**, 3829–3849.
  47. Sekine, S.-i., Nureki, O., Vassilyev, D. G., Bernier, S., Chênevert, R., LaPointe, J. & Yokoyama, S. (2002). Structural basis for the tRNA-dependent catalytic activation of glutamyl-tRNA synthetase. *EMBO J.* In press.
  48. Cusack, S., Yaremchuk, A. & Tukalo, M. (2000). The 2 Å crystal structure of leucyl-tRNA synthetase and its complex with a leucyl-adenylate analogue. *EMBO J.* **19**, 2351–2361.
  49. Delagoutte, B., Moras, D. & Cavarelli, J. (2000). tRNA aminoacylation by arginyl-tRNA synthetase: induced conformations during substrates binding. *EMBO J.* **19**, 5599–5610.
  50. Schmitt, E., Moulinier, L., Fujiwara, S., Imanaka, T., Thierry, J.-C. & Moras, D. (1998). Crystal structure of aspartyl-tRNA synthetase from *Pyrococcus kodakaraensis* KOD: archaeon specificity and catalytic mechanism of adenylate formation. *EMBO J.* **17**, 5227–5237.
  51. Serre, L., Verdon, G., Choinowski, T., Hervouet, N., Risler, J.-L. & Zelwer, C. (2001). How methionyl-tRNA synthetase creates its amino acid recognition pocket upon L-methionine binding. *J. Mol. Biol.* **306**, 863–876.
  52. Onesti, S., Desogus, G., Brevet, A., Chen, J., Plateau, P., Blanquet, S. & Brick, P. (2000). Structural studies of lysyl-tRNA synthetase: conformational changes induced by substrate binding. *Biochemistry*, **39**, 12853–12861.
  53. Traut, T. W. (1994). Physiological concentrations of purines and pyrimidines. *Mol. Cell. Biochem.* **140**, 1–22.
  54. Choithia, C. (1974). Surface area and hydrophobic free energy. *Nature*, **248**, 338–339.
  55. Feuerstein, J., Goody, R. S. & Wittinghofer, A. (1987). Preparation and characterization of nucleotide-free and metal ion-free p21 "Apoprotein". *J. Biol. Chem.* **262**, 8455–8458.
  56. Fersht, A. R. (1998). *Structure and Mechanism in Protein Science*, W.H. Freeman and Company, New York, NY.
  57. Schramm, V. L. (1999). Enzymatic transition-state analysis and transition-state analogs. *Methods Enzymol.* **308**, 301–355.
  58. Cleland, W. W. & Northrup, D. B. (1999). Energetics of substrate binding, catalysis, and product release. *Methods Enzymol.* **308**, 3–48.
  59. Gerretana, B., Frey, P. A. & Cleland, W. W. (2001). Characterization of the transition-state structure of the reaction of kanamycin nucleotidyltransferase by heavy-atom kinetic isotope effects. *Biochemistry*, **40**, 2972–2977.
  60. Vorobjev, Y. N., Almagro, J. C. & Hermans, J. (1998). Discrimination between native and intentionally misfolded conformations of proteins: ES/IS, a new method for calculating conformational free energy

- that uses both dynamics simulations with an explicit solvent and an implicit solvent continuum model. *Proteins: Struct. Funct. Genet.* **32**, 399–413.
61. Vorobjev, Y. N. & Hermans, J. (1999). ES/IS, estimation of conformational free energy by combining dynamics simulations with explicit solvent with an implicit solvent continuum model. *Biophys. Chem.* **78**, 195–205.
  62. Vorobjev, Y. N. & Hermans, J. (2001). Free energies of protein decoys provide insight into determinants of protein stability. *Protein Sci.* **10**, 2498–2506.
  63. Srinivasan, J., Cheatham, T. E., III, Cieplak, P., Kollman, P. A. & Case, D. A. (1998). Continuum solvent studies of the stability of DNA, RNA, and phosphoramidate–DNA helices. *J. Am. Chem. Soc.* **120**, 9401–9409.
  64. Koshland, D. E. Jr (1959). Mechanisms of transfer enzymes. In *The Enzymes* (Boyer, P. D., Lardy, H. & Myrbäck, K., eds), vol. I, pp. 305–346, Academic Press, New York.
  65. Wyman, J. & Gill, S. J. (1990). *Binding and Linkage*, University Science Books, Mill Valley, CA.
  66. Houdusse, A., Szent-Györgi, A. G. & Cohen, C. (2000). Three conformational states of scallop myosin S1. *Proc. Natl Acad. Sci. USA*, **97**, 11238–11243.
  67. Abrahams, J. P., Leslie, A. G. W., Lutter, R. & Walker, J. E. (1994). Structure at 2.8 Å resolution of F1-ATPase from bovine heart mitochondria. *Nature*, **370**, 621–628.
  68. Goldsmith, E. J. (1996). Allosteric enzymes as models for chemomechanical energy transducing assemblies. *FASEB J.* **10**, 702–708.
  69. Joseph, D. R. & Muench, K. (1971). Tryptophanyl-transfer ribonucleic acid synthetase of *Escherichia coli*. I. Purification of the enzyme and of tryptophan transfer ribonucleic acid. *J. Biol. Chem.* **246**, 7602–7609.
  70. Schoenmakers, T. J. M., Visser, G. J., Flik, G. & Theuvsen, A. P. R. (1992). CHELATOR: an improved method for computing metal ion concentrations in physiological solutions. *Biocomputing*, **12**, 870–879.
  71. Boulin, C., Kempf, R., Koch, M. H. J. & McLaughlin, S. M. (1986). Data appraisal, evaluation and display for synchrotron radiation experiments: hardware and software. *Nucl. Instrum. Methods*, **A249**, 399–407.
  72. Dubuisson, J. M., Decamps, T. & Vachette, P. (1997). Improved signal-to-background ratio in small-angle X-ray scattering experiments with synchrotron radiation using an evacuated cell for solutions. *J. Appl. Crystallog.* **30**, 49–54.
  73. Guinier, A. & Fournet, G. (1955). *Small Angle Scattering of X-rays*, Wiley, New York.
  74. Wilkinson, L. (1987). SYSTAT, the System for Statistical Analysis. 2902 Central St., Evanston IL 60601.
  75. SAS (2000). *JMP*, 4th edit., SAS, Cary, NC.
  76. Carter, C. W., Jr (1988). Cloning heterologous genes into *E. coli* for enzyme production and crystal growth: problems of expression and microheterogeneity. *J. Cryst. Growth*, **90**, 168–179.
  77. Otwinowski, Z. & Minor, W. (1997). Processing of X-ray diffraction data collected in oscillation mode. *Methods Enzymol.* **276**, 307–326.
  78. Otwinowski, Z. (1993). Oscillation data reduction program. In *Data Collection and Processing* (Sawyer, L., Isaacs, N. & Bailey, S., eds), pp. 80–86, Science and Engineering Research Council, Daresbury Laboratory, Daresbury, UK.
  79. French, G. S. & Wilson, K. S. (1978). On the treatment of negative intensity observations. *Acta Crystallog. sect. A*, **34**, 517–525.
  80. Howell, L. & Smith, D. (1992). Identification of heavy-atom derivatives by normal probability methods. *J. Appl. Crystallog.* **25**, 81–86.
  81. Collaborative Computing Project Number 4 (1991). *The SRC(UK) Collaborative Computing Project No 4: A Suite of Programs for Protein Crystallography*, Daresbury Laboratory, Daresbury, UK.
  82. Navaza, J. (1997). AMoRe: an automated molecular replacement package. *Methods Enzymol.* **276**, 581–594.
  83. National Laboratory for High Energy Physics. (1989). KEK report 88-14. Sasaki, S.
  84. Doublé, S. & Carter, C. W. Jr (1992). Preparation of selenomethionyl protein crystals. In *Crystallization of Proteins and Nucleic Acids, A Practical Approach* (Ducruix, A. & Giegé, R., eds), pp. 311–317, Oxford University Press, Oxford, UK.
  85. Abrahams, J. P. & Leslie, A. G. W. (1996). Methods used in the structure determination of bovine mitochondrial F1 ATPase. *Acta Crystallog. sect. D*, **52**, 30–42.
  86. Read, R. J. (1986). Improved Fourier coefficients for maps using phases from partial structures with errors. *Acta Crystallog. sect. A*, **42**, 140–149.
  87. Kleywegt, G. A. & Jones, T. A. (1996). Efficient rebuilding of protein structures. *Acta Crystallog. sect. D*, **52**, 826–828.
  88. Brünger, A. T. & Rice, L. M. (1997). Crystallographic refinement by simulated annealing: methods and applications. *Methods Enzymol.* **277**, 243–269.
  89. Irwin, J. & Bricogne, G. (1996). A test of maximum-likelihood refinement of macromolecular structures with Buster and TNT. *Acta Crystallog. sect. A*, **525**, C-86.
  90. Roversi, P., Blanc, E., Vornrhein, C., Evans, G. & Bricogne, G. (2000). Modelling prior distributions of atoms for macromolecular refinement and completion. *Acta Crystallog. sect. D*, **56**, 1316–1323.
  91. Di Cera, E., Guinto, E. R., Vindigni, A., Dang, Q. D., Ayala, Y. M., Wuyi, M. & Tulinsky, A. (1995). The Na<sup>+</sup> binding site of thrombin. *J. Biol. Chem.* **270**, 22089–22092.
  92. Kraulis, P. J. (1991). MOLSCRIPT: a program to produce both detailed and schematic plots of protein structures. *J. Appl. Crystallog.* **24**, 946–950.
  93. Esnouf, R. M. (1997). *J. Mol. Graph.* **15**, 132–134.
  94. Merrit, E. A. & Murphy, M. E. P. (1994). Raster3D version 2.0. A program for photorealistic molecular graphics. *Acta Crystallog. sect. D*, **50**, 869–873.
  95. Cleland, W. W. (1970). Steady state kinetics. In *The Enzymes* (Boyer, P., ed.), vol. II, pp. 1–65, Academic Press, New York.
  96. Cole, F. X. & Schimmel, P. (1970). *Biochemistry*, **9**, 480–489.

Edited by D. Rees

(Received 12 April 2002; received in revised form 7 October 2002; accepted 10 October 2002)